Deletion of both centrin 2 (CETN2) and CETN3 destabilizes the distal connecting cilium of mouse photoreceptors

Received for publication, October 19, 2018, and in revised form, January 9, 2019 Published, Papers in Press, January 15, 2019, DOI 10.1074/jbc.RA118.006371

Guoxin Ying[‡1], **Jeanne M. Frederick**[‡], **and Wolfgang Baehr**[‡§¶2]

From the [‡]*Department of Ophthalmology, University of Utah Health Science Center, Salt Lake City, Utah 84132, the* [§]*Department of Neurobiology and Anatomy, University of Utah, Salt Lake City, Utah 84112, and the* [¶]*Department of Biology, University of Utah, Salt Lake City, Utah 84132*

Edited by Henrik G. Dohlman

Centrins (CETN1–4) are ubiquitous and conserved EF-hand–family Ca^{2+}-binding proteins associated with the centrosome, basal body, and transition zone. Deletion of CETN1 or CETN2 in mice causes male infertility or dysosmia, respectively, without affecting photoreceptor function. However, it remains unclear to what extent centrins are redundant with each other in photoreceptors. Here, to explore centrin redundancy, we generated *Cetn3*$^{GT/GT}$ single-knockout and *Cetn2*$^{-/-}$;*Cetn3*$^{GT/GT}$ double-knockout mice. Whereas the *Cetn3* deletion alone did not affect photoreceptor function, simultaneous ablation of *Cetn2* and *Cetn3* resulted in attenuated scotopic and photopic electroretinography (ERG) responses in mice at 3 months of age, with nearly complete retina degeneration at 1 year. Removal of CETN2 and CETN3 activity from the lumen of the connecting cilium (CC) destabilized the photoreceptor axoneme and reduced the CC length as early as postnatal day 22 (P22). In *Cetn2*$^{-/-}$;*Cetn3*$^{GT/GT}$ double-knockout mice, spermatogenesis-associated 7 (SPATA7), a key organizer of the photoreceptor-specific distal CC, was depleted gradually, and CETN1 was condensed to the mid-segment of the CC. Ultrastructural analysis revealed that in this double knockout, the axoneme of the CC expanded radially at the distal end, with vertically misaligned outer segment discs and membrane whorls. These observations suggest that CETN2 and CETN3 cooperate in stabilizing the CC/axoneme structure.

Centrins belong to a group of ~350 eukaryotic signature proteins that are highly conserved and thought to be critical for eukaryote structure and function (1). Centrins are ~20-kDa Ca^{2+}-binding proteins of the EF-hand superfamily, where two pairs of EF-hand motifs at each N- and C-terminal region, connected by a helical rod, form a dumbbell-shaped protein (2). Centrins localize to the centriole distal lumen, the pericentriolar matrix, and the transition zone (TZ)[3] of primary cilia (3–5). Although it is well-established that centrins in lower eukaryotes are required for centriole replication and positioning (6–8), the requirement of centrins during vertebrate centriole duplication is controversial (9–14). A recent study found that CETN2 positively regulates primary ciliogenesis by removing the centriole cap protein CP110 *in vitro* (15). Morpholino-based depletion of *Cetn2* in zebrafish embryos also leads to cilia loss in multiple tissues (16).

There are four centrin genes (*CETN1–4*) in mammalian genomes that encode the Vfl2 (*Chlamydomonas* centrin)-like CETN1, -2, and -4 and the budding yeast CDC31-related CETN3 (17, 18). CETN1 is highly expressed in sperm and ciliated cells (19). CETN2 and CETN3 are expressed ubiquitously in all somatic cells (4, 20), and CETN4 is expressed in ciliated tissues (21). Knockout of *Cetn1* in mouse causes male infertility because of centriole rearrangement deficiency at a late stage of spermiogenesis (22). Knockout of *Cetn2* in mouse also leads to dysosmia and hydrocephalus as a result of impaired olfactory ciliary trafficking of adenylate cyclase III (ACIII) and cyclic nucleotide-gated channel α2 (CNGA2) and disrupted planar polarity of ependymal cilia, respectively (23). In germline knockouts of CETN1 and CETN2 and in CETN1/CETN2 double knockouts, rod and cone photoreceptors develop normally and exhibit normal function (23). A possible explanation for this is the functional centrin redundancy. CETN1–3 localize to the lumen of the axoneme of the photoreceptor CC (24, 25), which connects the inner segment (IS) to the outer segment (OS). Each connecting cilium is an elongated TZ of ~1.1 μm length (compared with 0.2–0.5 μm in primary cilia) consisting of an array of nine microtubule doublets emanating from the basal body. It was recently found that the CC can be divided into two domains, a proximal CC corresponding to the TZ of primary cilia and a distal photoreceptor-specific CC that supports the very large photosensitive OS (26).

Our results show that removal of both CETN2 and CETN3 from the CC lumen leads to a widening of the distal CC microtubule doublet array similar to observations in a *Spata7* knockout

This work was supported by National Institutes of Health Grants 1R01 EY08123 and 1R01 EY019298 (to W. B.) and 1P30 EY014800-039003 from the NEI (NEI core grant). This work also was supported by unrestricted grants to the University of Utah Dept. of Ophthalmology from Research to Prevent Blindness (RPB, New York). The authors declare that they have no conflicts of interest with the contents of this article. The content is solely the responsibility of the authors and does not necessarily represent the official views of the National Institutes of Health.

[1] To whom correspondence may be addressed. E-mail: g.ying@utah.edu.

[2] Recipient of an RPB Senior Investigator award and an RPB Nelson Trust award. To whom correspondence may be addressed. E-mail: wbaehr@hsc.utah.edu.

[3] The abbreviations used are: TZ, transition zone; IS, inner segment; OS, outer segment; GT, gene-trapped; ERG, electroretinography; ONL, outer nuclear layer; DAPI, 4′,6-diamidino-2-phenylindole; CC, connecting cilium; DCC, distal connecting cilium; 3m, 3-month-old; P22, postnatal day 22; Ac, acetylated; ES, embryonic stem (cell); ANOVA, analysis of variance; OCT, optimal cutting temperature; GC1, guanylate cyclase 1; PNA, peanut agglutinin; ROS, rod outer segment; cd, candela(s); FRT, flippase recognition target; RPGRIP, RPGR-interacting protein; RPGR, retinitis pigmentosa GTPase regulator.

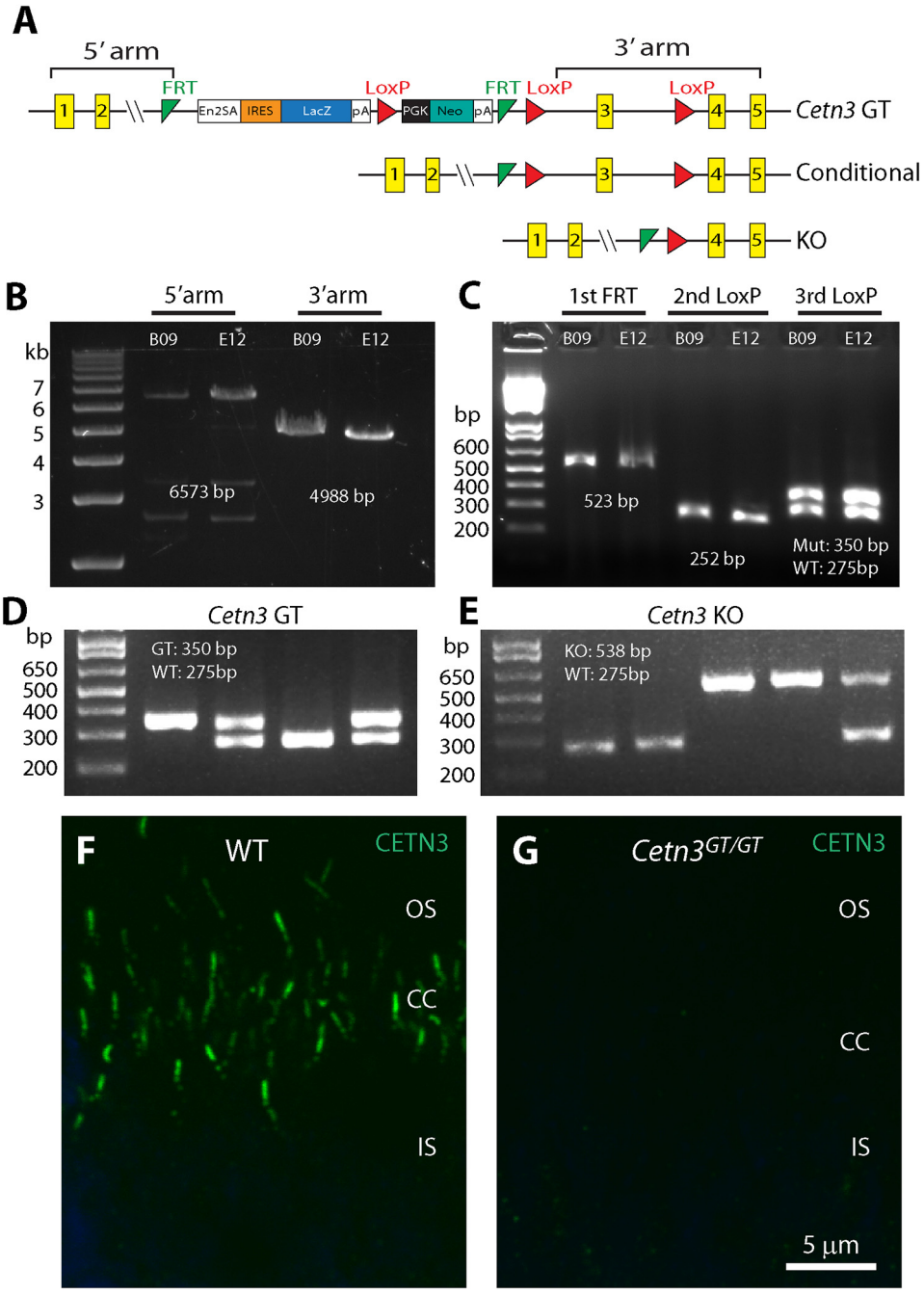

Figure 1. Generation of *Cetn3*$^{GT/GT}$ and *Cetn3*$^{-/-}$ mice. *A*, schematic representation of the mouse *Cetn3* gene trap and conditional and knockout alleles. The mouse *Cetn3* gene consists of 5 exons (*yellow rectangles*). The En2SA-IRES-LacZ-pGK-Neo GT cassette, which is flanked by two FRT sites (*green triangles*), is inserted into intron 2 by homologous recombination. Exon 3 is flanked by two LoxP sites (*red triangles*). *B* and *C*, PCR genotyping of 3′ and 5′ recombination arms (*B*) and 1st FRT, 2nd LoxP, and 3rd LoxP sites in two ES cell clones, B09 and E12 (*C*). *D* and *E*, PCR genotyping result of one litter each of *Cetn3*$^{GT/+}$ × *Cetn3*$^{GT/+}$ (*D*) and *Cetn3*$^{+/-}$ × *Cetn3*$^{+/-}$ (*E*) pups. Primer sequences are listed in Table 2. *F* and *G*, immunohistochemistry of WT (*F*) and *Cetn3*$^{GT/GT}$ (*G*) retina cryosections incubated with anti-CETN3 antibody. Signal attributable to CETN3 is present in CC and basal bodies of WT photoreceptors (*left*) but absent from *Cetn3*$^{GT/GT}$ photoreceptors (*right*). *Scale bar*: 5 μm.

(26). CETN1 accumulates at the mutant CC center, presumably stabilizing the proximal CC. Weakening of the distal CC axoneme leads to misalignment of discs, formation of membrane whorls, OS malformation, and progressive photoreceptors degeneration.

Results

Generation of Cetn3 KO mouse

The mouse *Cetn3* gene consists of 5 exons. We generated gene-trapped *Cetn3* mice (*Cetn3*$^{GT/GT}$) in which FRT sites flanked the gene trap cassette inserted into intron 2 and LoxP sites flanked exon 3 (Fig. 1*A*). The presence of the gene trap truncates CETN3 after amino acid 52, producing a nonfunctional N-terminal fragment containing the first EF-hand motif (EF1). Correct gene targeting was confirmed by PCR amplification of 5′ and 3′ recombination arms, in addition to FRT and LoxP sites and DNA sequencing (Fig. 1, *B* and *C*). *Cetn3*$^{GT/GT}$ mice (Fig. 1*D*) were crossed with *Flp* mice to remove the GT cassette, generating floxed mice (*Cetn3*$^{f/f}$), which were subse-

Table 1
Pup counts for centrin KO lines

Total litters counted are 17, 47, and 43 for *Cetn3, Cetn2,* and *Cetn2/3* lines, respectively. *For Cetn2 and Cetn2/3 lines, the ratio represents male KO ($Cetn2^{-/Y}$ and $Cetn2^{-/Y}$;$Cetn3^{GT/GT}$) of total male pups.

Breeding scheme	Pup counts	Ratio	Mendelian ratio	Litter size
Female × male	*KO/Total*	*KO/Total*	*KO/Total*	
$Cetn3^{GT/+} \times Cetn3^{GT/+}$	29/116	25%	50%	6.8
$Cetn2^{+/-} \times Cetn2^{+/Y}$	62/146*	42.5%	50%	6.7
$Cetn2^{+/-}$;$Cetn3^{GT/GT} \times Cetn3^{GT/GT}$	38/130*	29.2%	50%	5.5

quently mated with a CMV-Cre line to delete exon 3 (Fig. 1*E*), thus truncating CETN3 in exon 4 in a different frame. Both the $Cetn3^{GT/GT}$ and $Cetn3^{-/-}$ mice were born in a Mendelian ratio (29 knockouts of 116 total pups (Table 1)), were viable and fertile and did not reveal syndromic ciliopathy. As reported (24), CETN3 protein localized to the wildtype (WT) photoreceptor CC and both centrioles (Fig. 1*F*). In $Cetn3^{GT/GT}$ (Fig. 1*G*) and $Cetn3^{-/-}$ (not shown) photoreceptors, CETN3 was undetectable, thereby confirming the null allele in each line.

Retina function of CETN3-deficient mice was evaluated by electroretinography (ERG) (Fig. 2, *A–C*). Eight-month-old (8m) $Cetn3^{+/+}$, $Cetn3^{GT/+}$, and $Cetn3^{GT/GT}$ mice displayed comparable scotopic a-wave (Fig. 2*A*), scotopic b-wave (Fig. 2*B*), and photopic b-wave (Fig. 2*C*) amplitudes at every light intensity tested. In the 1-year-old (12m) $Cetn3^{GT/GT}$ retina, all examined rod and cone OS proteins (including rhodopsin, guanylate cyclase 1 (GC1), PDE6, CNGA1/A3, ROM1, and S- and M-opsins) were localized correctly, the same as in the heterozygous controls (Fig. 2*D*). The ONL thickness and cone density of 26m $Cetn3^{-/-}$ and $Cetn3^{+/+}$ retina cryosections were comparable and exhibited no signs of degeneration (Fig. 2*E*). These results indicate that, as found in $Cetn1^{-/-}$ and $Cetn2^{-/-}$ single knockouts, CETN3 is dispensable for mouse photoreceptor development and function.

$Cetn2^{-/-}$;$Cetn3^{GT/GT}$ mice are born in non-Mendelian ratios

Mouse CETN3 and CETN2 belong to two distinct centrin subfamilies (6) but are highly similar in amino acid sequence (51% identity and 81% similarity). To investigate the functional redundancy between these two centrins, we generated $Cetn2^{-/-}$;$Cetn3^{GT/GT}$ double knockout mice (see "Experimental procedures"). In our breeding scheme of $Cetn2^{+/-}$;$Cetn3^{GT/GT}$ females mated with $Cetn3^{GT/GT}$ males, we noticed that the ratio of $Cetn2^{-/Y}$;$Cetn3^{GT/GT}$ (29.2%, 38 of 130 total male pups) was below the expected Mendelian ratio of 50% (Table 1), indicating that some $Cetn2^{-/Y}$;$Cetn3^{GT/GT}$ male embryos did not survive prenatal development. We reported previously that $Cetn2^{-/-}$ pups were born at a Mendelian ratio (23); after carefully assessing 47 litters, we found that indeed $Cetn2^{-/-}$ pups were also born slightly below its predicted Mendelian ratio (62 of 146, 42.5%) (Table 1). The average litter size of the $Cetn2^{-/Y}$;$Cetn3^{GT/GT}$ line (5.5) was smaller than observed in either the $Cetn3^{GT/GT}$ (6.8) or $Cetn2^{-/-}$ (6.7) line.

$Cetn2^{-/-}$;$Cetn3^{GT/GT}$ mice exhibit progressive retina degeneration

$Cetn2^{-/-}$;$Cetn3^{GT/GT}$ pups survived to adulthood and showed syndromic ciliopathy, as observed in $Cetn2^{-/-}$ mice, including dysosmia and hydrocephalus (not shown). To identify a retina phenotype, we examined $Cetn2^{-/-}$;$Cetn3^{GT/GT}$ retina morphology at 1, 3, and 13 months with anti-GC1 mAb (an OS marker) and DAPI (4′, 6-diamidino-2-phenylindole) as a nuclear marker (Fig. 3). We found that at 1 month, the $Cetn2^{-/-}$;$Cetn3^{GT/GT}$ ONL thickness and OS length were comparable with that of WT controls in dorsal and ventral retina (Fig. 3*A*, *first* and *second column*). By 3 months of age, the $Cetn2^{-/-}$;$Cetn3^{GT/GT}$ ONL thickness and OS length were greatly reduced, and the phenotype was more severe in the dorsal retina than in the ventral retina (Fig. 3*A*, *third column*). By 13 months, only one layer of ONL nuclei remained at the dorsal retina with residual OS/IS, as compared with 4–5 layers of nuclei at the ventral ONL. The ventral retina was much more stable, displaying OS of half-normal length (Fig. 3*A*, fourth column). We found a consistent reduction of ONL thickness and OS lengths across 3 month-old $Cetn2^{-/-}$;$Cetn3^{GT/GT}$ retinas (Fig. 3, *B* and *C*). The $Cetn3^{GT/GT}$ central retina displayed about 10 rows of nuclei (45–50-μm thickness) at either the dorsal or ventral areas, whereas the $Cetn2^{-/-}$;$Cetn3^{GT/GT}$ retina had 6–7 rows of nuclei (30–35 μm) at the ventral retina and 4–5 rows of nuclei (20–25 μm) at the dorsal retina (Fig. 3*B*). $Cetn3^{GT/GT}$ central retinas had an average OS length of 15–25 μm (both dorsal and ventral), whereas the OS length of the $Cetn2^{-/-}$;$Cetn3^{GT/GT}$ ventral retina was reduced to 10–15 μm and the dorsal peripheral retina to 5–10 μm (Fig. 3*C*). At 1 month, the ONL thickness and OS length of $Cetn2^{-/-}$;$Cetn3^{GT/GT}$ was comparable with the $Cetn3^{GT/GT}$ control at both the dorsal and ventral retina (Fig. 3, *D* and *E*). These results show that lack of CETN2 and CETN3 caused a slow photoreceptor degeneration beginning after ~1 month of age and nearing completion in the dorsal retina at 1 year.

ERG reveals $Cetn2^{+/-}$;$Cetn3^{GT/GT}$ haploinsufficiency

Consistently, 3-month-old $Cetn2^{-/-}$;$Cetn3^{GT/GT}$ mice had a significantly reduced scotopic ERG response compared with littermate $Cetn3^{GT/GT}$ controls, whereas $Cetn2^{+/-}$;$Cetn3^{GT/GT}$ littermates showed an intermediate ERG response at multiple light intensities (Fig. 4*A*). Quantification of scotopic ERG a-waves revealed that $Cetn2^{-/-}$;$Cetn3^{GT/GT}$ mice produced significantly smaller amplitudes compared with $Cetn2^{+/-}$;$Cetn3^{GT/GT}$ littermates (Fig. 4*B*). Scotopic b-wave amplitudes showed a similar reduction in $Cetn2^{-/-}$;$Cetn3^{GT/GT}$ mice compared with $Cetn2^{+/-}$;$Cetn3^{GT/GT}$, $Cetn2^{-/-}$;$Cetn3^{GT/GT}$, and $Cetn3^{GT/GT}$ mice at all light intensities (Fig. 4*C*). Although both scotopic a-wave and b-wave amplitudes were reduced in $Cetn2^{+/-}$;$Cetn3^{GT/GT}$ compared with $Cetn3^{GT/GT}$, the reductions were statistically insignificant ($p > 0.1$) except for the b-wave amplitude at 1.4 log cd s/m^2 ($p < 0.05$), probably because of the small group number ($n = 5$) and relatively large data variation among samples. We observed similar cone photopic ERG reduction in $Cetn2^{-/-}$;$Cetn3^{GT/GT}$ mice (Fig. 4*D*). In quantification, $Cetn2^{-/-}$;$Cetn3^{GT/GT}$ mice had significantly smaller photopic b-wave amplitudes compared with $Cetn2^{+/-}$;$Cetn3^{GT/GT}$ and $Cetn3^{GT/GT}$ (Fig. 4*E*). A small but insignificant ($p > 0.5$) reduction of scotopic and photopic ERG in 1-month-old $Cetn2^{-/-}$;$Cetn3^{GT/GT}$ mice relative to $Cetn3^{GT/GT}$ littermate controls was observed (Fig. 4*F* and not shown).

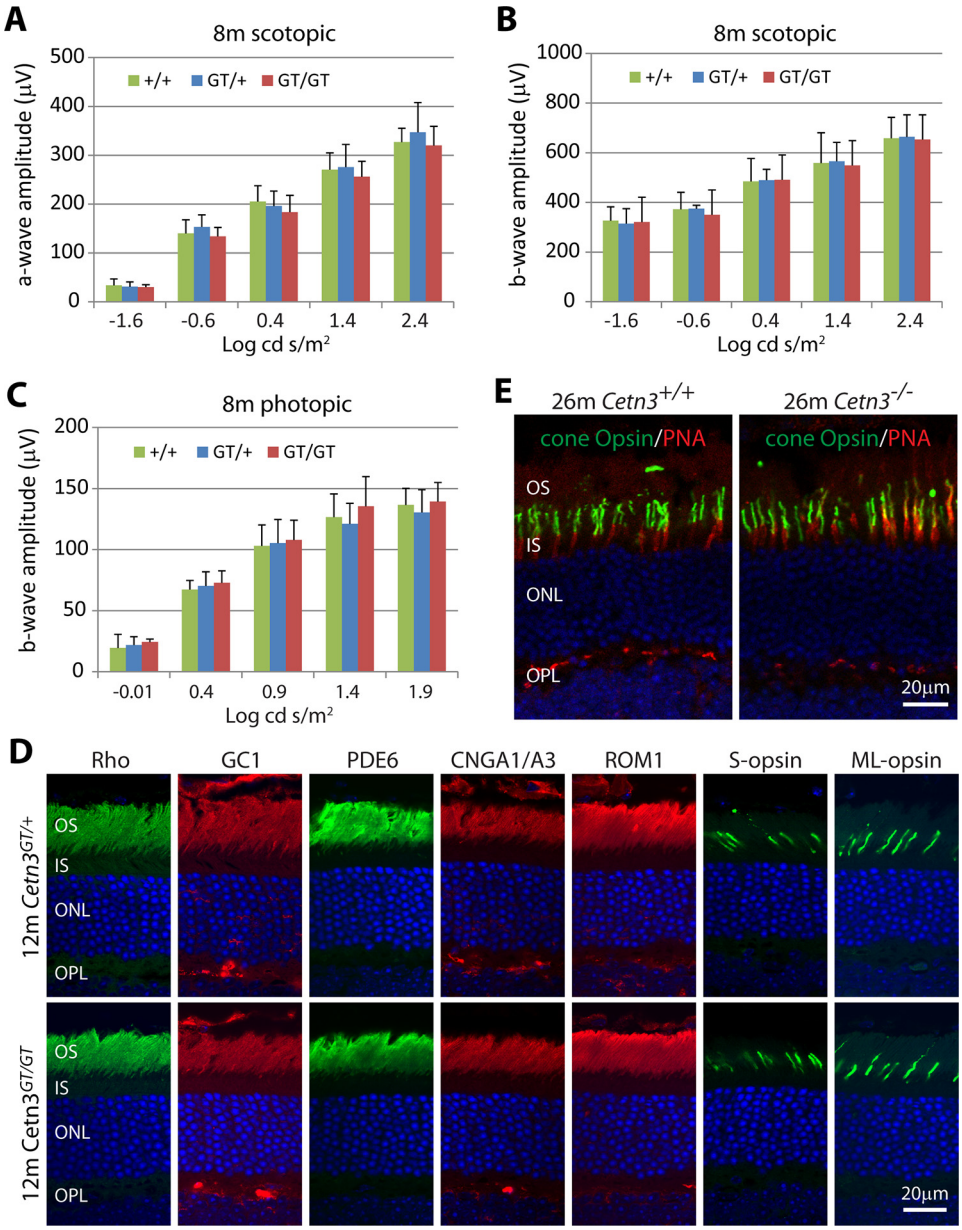

Figure 2. *Cetn3* mutant photoreceptors display normal ERGs and ciliary trafficking. *A–C*, scotopic ERG a-wave amplitude (*A*) and b-wave amplitude (*B*) at −1.6, −0.6, 0.4, 1.4, and 2.4 log cd s/m^2 light intensity and photopic b-wave amplitude (*C*) at −0.01, 0.4, 0.9, 1.4, and 1.9 log cd s/m^2 from 8-month-old (*8m*) *Cetn3*$^{+/+}$, *Cetn3*$^{GT/+}$, and *Cetn3*$^{GT/GT}$ mice. Scotopic a-wave amplitudes are (in μV) 34, 140, 205, 271, and 326 for +/+; 31, 154, 196, 276, and 347 for GT/+; 31, 134, 184, 256, and 320 for GT/GT; and scotopic b-wave amplitudes are (in μV) 326, 373, 485, 559, and 658 for +/+; 314, 375, 489, 566, and 664 for GT/+; 321, 350, 492, 594, and 653 for GT/GT at −1.6, −0.6, 0.4, 1.4, and 2.4 log cd s/m^2, respectively. Photopic b-wave amplitudes are: 22, 70, 105, 121, and 131 for +/+; 25, 73, 108, 136, and 139 for GT/+; 20, 67, 103, 127, and 137 for GT/GT at −0.01, 0.4, 0.9, 1.4, and 1.9 log cd s/m^2, respectively, No significant difference was detected among the three genotypes. Shown are mean ± S.D., $n \geq 5$ for each group; one-way ANOVA; $p > 0.5$. *D*, localization of OS markers, rhodopsin, GC1, PDE6, CNGA1/A3, ROM1, and S- and ML-opsin in 12-month-old *Cetn3*$^{GT/+}$ (*top row*) and *Cetn3*$^{GT/GT}$ (*bottom row*) retina sections. *E*, cone opsin (combined S- and ML-antibodies) immunostaining of 26-month-old *Cetn3*$^{+/+}$ and *Cetn3*$^{-/-}$ retina sections, contrasted with PNA (*red*, for cone sheaths) and DAPI (*blue*, for nuclei). No reduction of ONL thickness or cone density was noticed in the *Cetn3*$^{-/-}$ mutant. *Scale bars*: 20 μm.

OS protein trafficking proceeds in the absence of CETN2 and CETN3

Immunolabeling with antibodies directed against phototransduction proteins showed normal localizations of rod or cone OS proteins (rhodopsin, GC1, PDE6, CNGA1/A3, and S- and M-opsins) in 3-month-old *Cetn2*$^{-/-}$;*Cetn3*$^{GT/GT}$ retinas despite ongoing photoreceptor degeneration (Fig. 5, *A* and *B*). A notable observation was the enlargement of cone OS in *Cetn2*$^{-/-}$;*Cetn3*$^{GT/GT}$ mice (*arrows* in Fig. 5*B*); WT cone outer segments labeled with anti-cone arrestin taper distally (Fig. 5*C*), whereas a fraction of the *Cetn2*$^{-/-}$;*Cetn3*$^{GT/GT}$ cone OS was swollen to triple diameter (Fig. 5*D*). The swelling (up to 3 μm in diameter) was even more obvious when sections were immunolabeled with anti-M–opsin (Fig. 5*E*).

Proximal Cetn2$^{-/-}$*;Cetn3*$^{GT/GT}$ *axonemes reveal decreased RP1 immunolabeling*

To gain insight into the mechanisms underlying the *Cetn2*$^{-/-}$;*Cetn3*$^{GT/GT}$ photoreceptor degeneration, we immunolabeled predegenerate retina sections with antibodies directed against

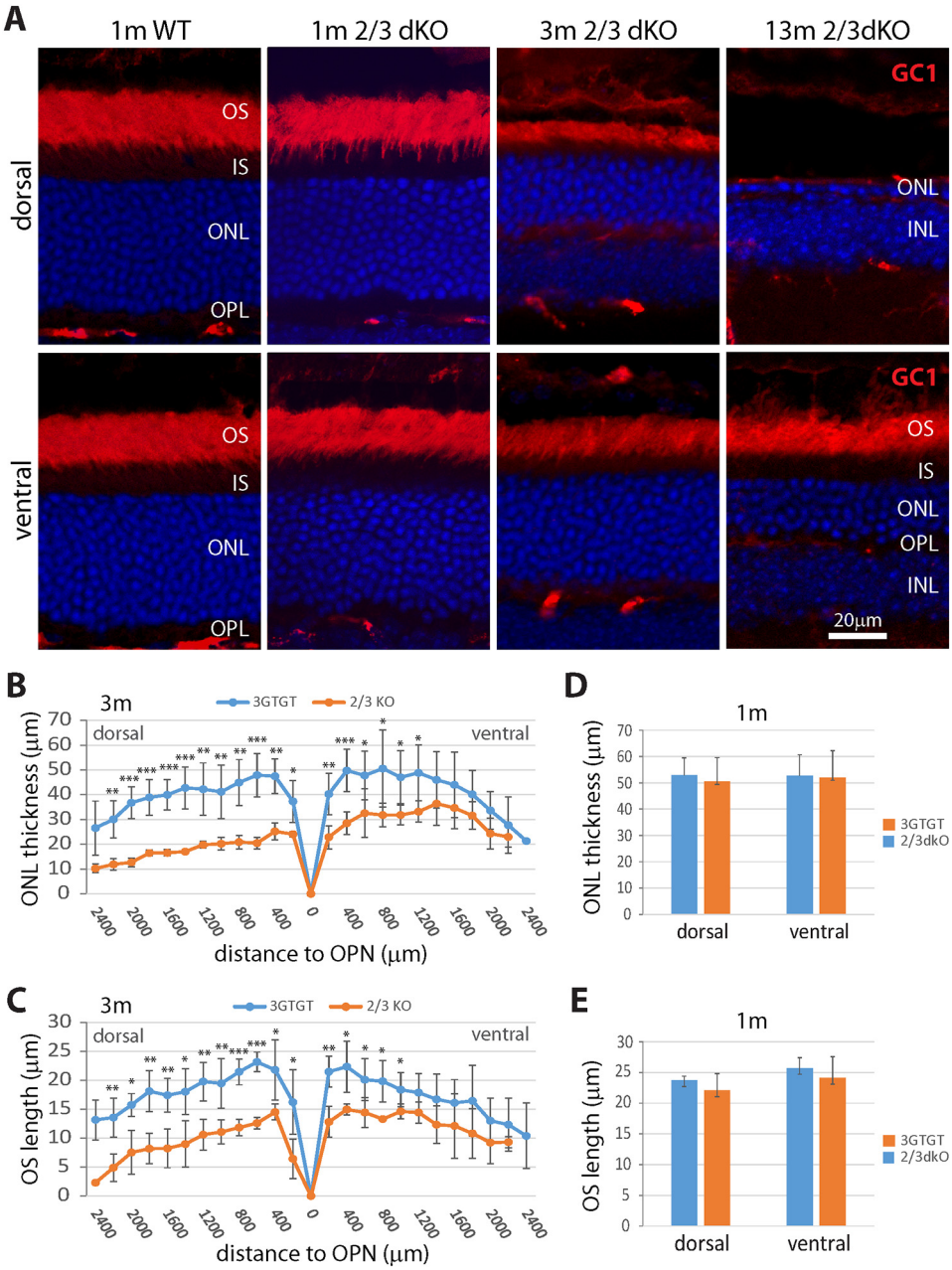

Figure 3. *Cetn2*$^{-/-}$;*Cetn3*$^{GT/GT}$ mice undergo progressive photoreceptor degeneration. *A*, immunolabeling of GC1 in central dorsal (*top row*) and ventral (*bottom row*) retina sections of WT and *Cetn2*$^{-/-}$;*Cetn3*$^{GT/GT}$ mice at the indicated ages. Note that the gradual reduction of ROS length and ONL thickness in mutants is more severe dorsally; blood vessel labeling is nonspecific, as IS4 is a mAb. *Scale bar*: 20 μm. *B* and *C*, ONL thickness (*B*) and ROS length (*C*) across the retinas of 3-month-old *Cetn3*$^{GT/GT}$ and *Cetn2*$^{-/-}$;*Cetn3*$^{GT/GT}$ mice. Data points were taken every 200 μm from the optic nerve head (*OPN*) (position 0) toward the retina periphery. *D* and *E*, ONL thickness (*D*) and ROS length (*E*) of dorsal and ventral central retinas at 1 month. Shown are mean ± S.D., $n = 5$ for *Cetn3*$^{GT/GT}$ and $n = 4$ for *Cetn2*$^{-/-}$;*Cetn3*$^{GT/GT}$; one-way ANOVA; *, $p < 0.05$; **, $p < 0.01$; ***, $p < 0.001$.

axoneme and ciliary markers. The length of proximal axonemes labeled by RP1 (retinitis pigmentosa 1 protein), a microtubule-associated protein (27), was slightly but significantly reduced in P22 *Cetn2*$^{-/-}$;*Cetn3*$^{GT/GT}$ photoreceptors compared with those of the *Cetn3*$^{GT/GT}$ littermate controls (Fig. 6, *A–D*). The average length of the RP1-responsive *Cetn3*$^{GT/GT}$ proximal axoneme was 4.58 ± 0.92 μm and for the *Cetn2*$^{-/-}$;*Cetn3*$^{GT/GT}$ axoneme 3.92 ± 0.87 μm (Fig. 6*G*). By 3 months, the reduction was more obvious (Fig. 6, *E* and *F*), with the *Cetn2*$^{-/-}$;*Cetn3*$^{GT/GT}$ RP1 length measured as 2.49 ± 0.55 μm, 56% of the *Cetn3*$^{GT/GT}$ controls (4.41 ± 0.67 μm) (Fig. 6*G*). These observations indicate that loss of CETN2 and -3 progressively reduced RP1 decoration of the proximal axoneme microtubules.

CETN1 accumulation in the Cetn2$^{-/-}$;*Cetn3*$^{GT/GT}$ *central CC*

Double immunolabeling with anti-CEP290 and anti-CETN1 antibodies showed a nearly full overlap of CEP290 and CETN1 along the entire P25 WT CC (98%, Fig. 6, *H–J* and *T*). In P25 *Cetn2*$^{-/-}$;*Cetn3*$^{GT/GT}$ photoreceptors, CEP290 labels the full-length CC, but CETN1 appears to accumulate at the CC center with variable depletion occurring at the proximal and distal

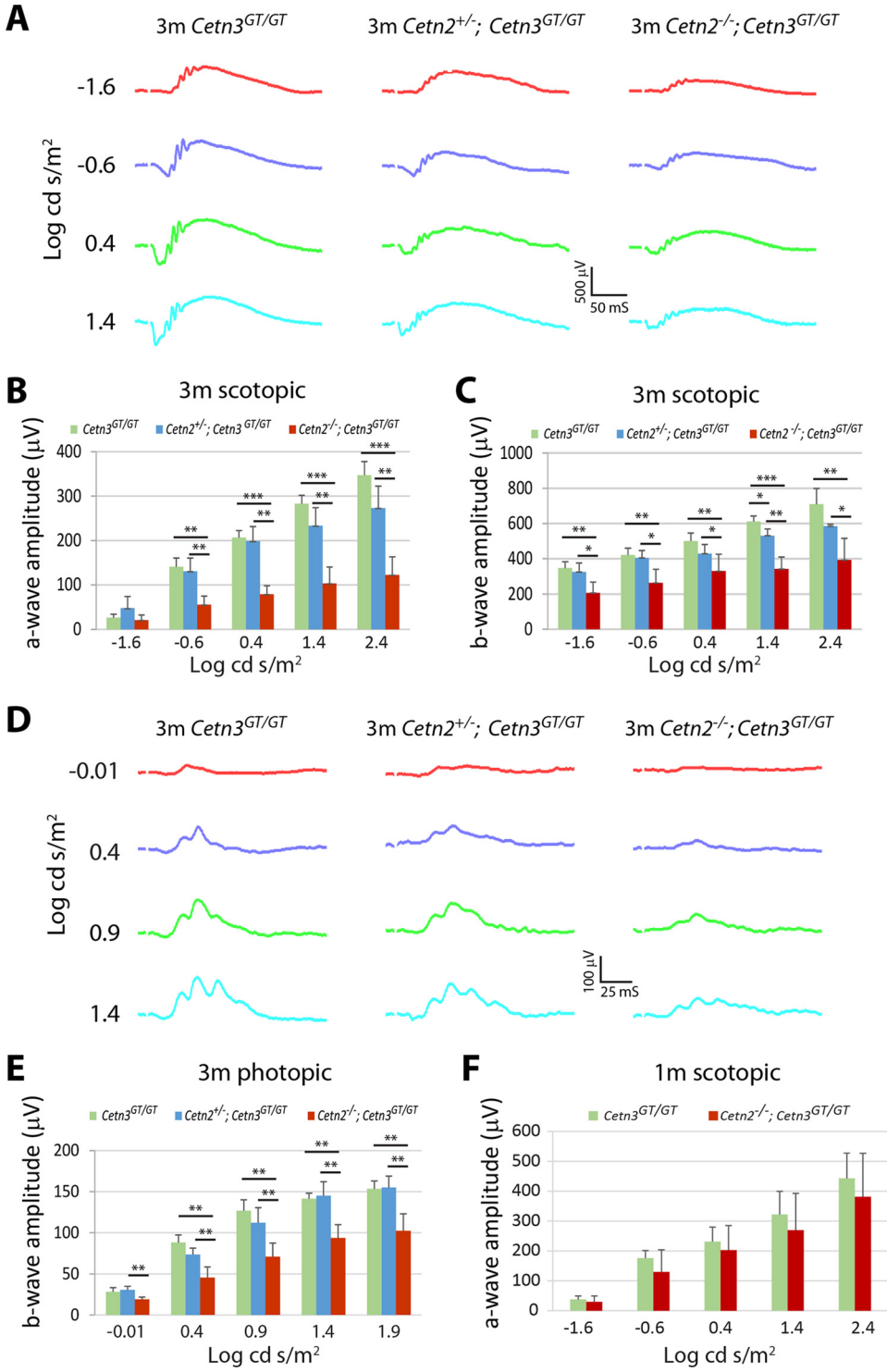

Figure 4. *Cetn2*$^{-/-}$;*Cetn3*$^{GT/GT}$ retinas reveal attenuated ERG responses at 3 months. *A*, representative scotopic ERG traces at −1.6, −0.6, 0.4, and 2.4 log cd s/m^2 from 3-month-old *Cetn3*$^{GT/GT}$, *Cetn2*$^{+/-}$;*Cetn3*$^{GT/GT}$, and *Cetn2*$^{-/-}$;*Cetn3*$^{GT/GT}$ mice. *B*, scotopic a-wave amplitudes in *Cetn2*$^{-/-}$;*Cetn3*$^{GT/GT}$ (21, 56, 79, 103, and 123 μV) at −1.6, −0.6, 0.4, 1.4, and 2.4 log cd s/m^2, respectively, are significantly smaller than the corresponding amplitudes in *Cetn3*$^{GT/GT}$ controls (27, 141, 207, 282, and 347 μV) or *Cetn2*$^{+/-}$;*Cetn3*$^{GT/GT}$ (48, 131, 199, 233, and 273 μV). Shown are mean ± S.D.; **, $p < 0.01$, and ***, $p < 0.001$; $n = 5$, one-way ANOVA, except for −1.6 log cd s/m^2, $p > 0.5$. *C*, scotopic b-wave amplitudes of *Cetn2*$^{-/-}$;*Cetn3*$^{GT/GT}$ mice (207, 264, 330, 343, and 393 μV) at −1.6, −0.6, 0.4, 1.4, and 2.4 log cd s/m^2, respectively, are significantly smaller than corresponding amplitudes of *Cetn2*$^{+/-}$;*Cetn3*$^{GT/GT}$ (325, 406, 429, 531 and 585 μV), or *Cetn3*$^{GT/GT}$ (348, 421, 501, 612, and 709 μV). Shown are mean ± S.D.;**, $p < 0.01$, and ***, $p < 0.001$; $n = 5$, one-way ANOVA. *D*, representative photopic ERG traces at −0.01, 0.4, 0.9, and 1.4 log cd s/m^2 from 3-month-old *Cetn3*$^{GT/GT}$, *Cetn2*$^{+/-}$;*Cetn3*$^{GT/GT}$, and *Cetn2*$^{-/-}$;*Cetn3*$^{GT/GT}$ mice. *E*, photopic b-wave amplitudes at −0.01, 0.4, 0.9, 1.4, and 1.9 log cd s/m^2 of 3-month-old *Cetn2*$^{-/-}$;*Cetn3*$^{GT/GT}$ mice (19, 45, 71, 94, and 102 μV) are significantly smaller than those of *Cetn2*$^{+/-}$;*Cetn3*$^{GT/GT}$ mice (31, 74, 112, 145, and 155 μV) or of *Cetn3*$^{GT/GT}$ mice (28, 88, 127, 142, and 154 μV). Shown are mean ± S.D.; **, $p < 0.01$, and ***, $p < 0.001$; $n = 5$, one-way ANOVA. *F*, scotopic a-wave amplitudes at −1.6, −0.6, 0.4, 1.4, and 2.4 log cd s/m2 of 1-month-old *Cetn3*$^{GT/GT}$ mice (37, 176, 231, 322, and 443 μV) appear larger than those in *Cetn2*$^{-/-}$;*Cetn3*$^{GT/GT}$ mice (29, 126, 203, 269, and 381 μV), but the difference is not significant. Shown are mean ± S.D.; $p > 0.4$, $n \geq 5$ for each group, one-way ANOVA.

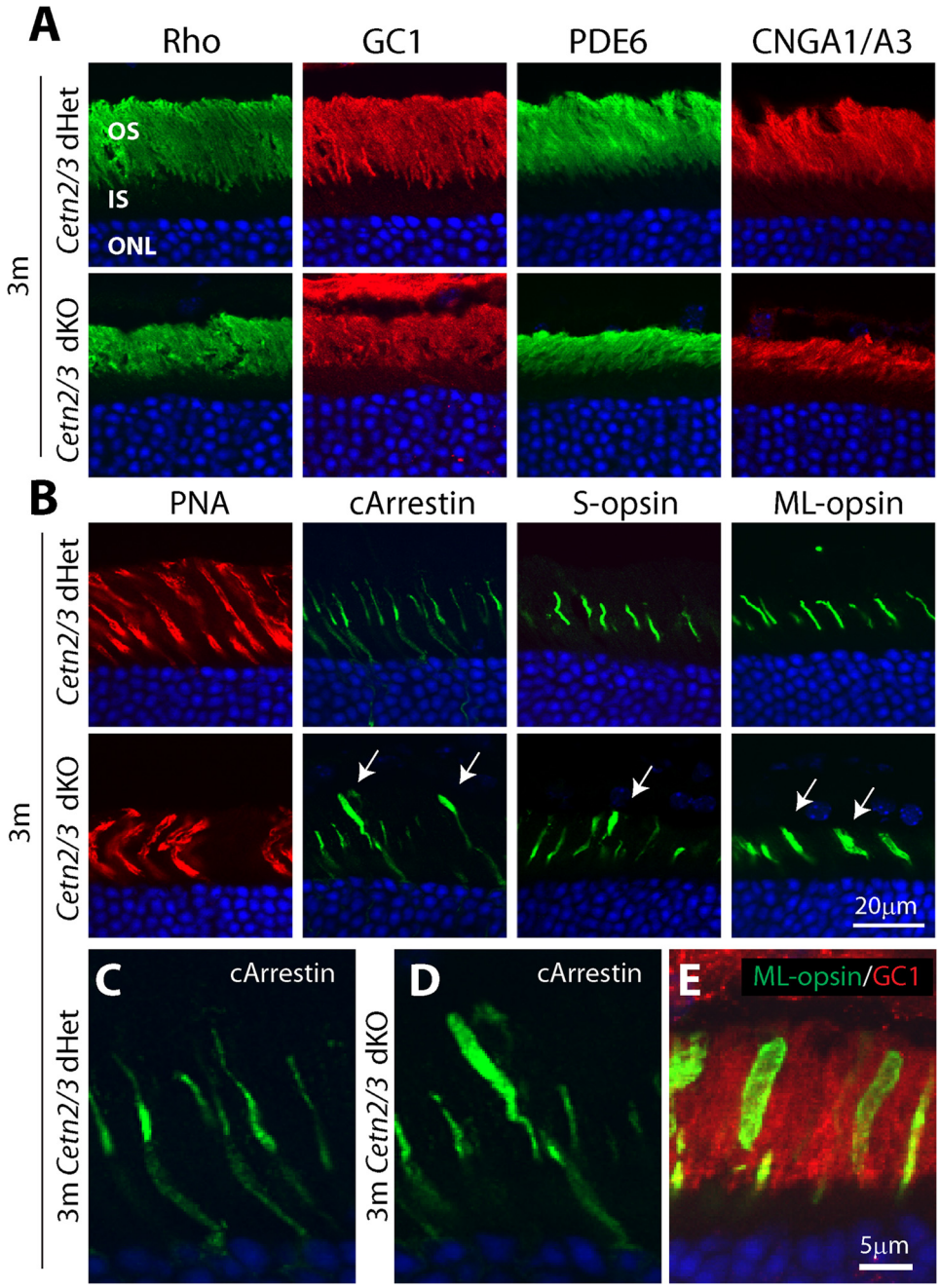

Figure 5. Normal rod and cone OS protein localization in *Cetn2*$^{-/-}$;*Cetn3*$^{GT/GT}$ photoreceptors. *A* and *B*, immunolocalization of rod OS proteins, rhodopsin, GC1, PDE6, and CNGA1/A3 (*A*) and of cone markers, PNA, cone arrestin, and S- and ML-opsins (*B*) in retina cryosections of 3-month-old *Cetn2*$^{+/-}$;*Cetn3*$^{GT/+}$ (*upper row*) *versus* *Cetn2*$^{-/-}$;*Cetn3*$^{GT/GT}$ (*lower row*) mice. Despite retina degeneration, no mislocalization of any OS protein was observed, but cone OS is enlarged in *Cetn2*$^{-/-}$;*Cetn3*$^{GT/GT}$ (*arrows* in *B*). *C* and *D*, closer view of cone arrestin staining of *Cetn2*$^{+/-}$;*Cetn3*$^{GT/+}$ cones (*C*) and *Cetn2*$^{-/-}$;*Cetn3*$^{GT/GT}$ cones (*D*). *E*, co-labeling of mutant retina with antibodies directed against ML-opsin and GC1 shows two swollen cones and a normal-size cone.

ends. We observed CC showing 36% CETN1 overlap with CEP290, CC showing 40% CETN1 depletion from the distal end (*arrows*), and CC showing 23% depletion from both the distal and proximal ends (*arrowheads*) (Fig. 6, *K–M* and *T*). By 3 months of age, CEP290 and CETN1 similarly overlap at the WT CC (98%, Fig. 6, *N–P* and *T*), whereas in *Cetn2*$^{-/-}$;*Cetn3*$^{GT/GT}$ CC, 67 and 28% of the CC were nonresponsive for CETN1 at the distal end (*arrows*) or from both the distal and proximal ends (*arrowheads*), respectively (Fig. 6, *Q–S* and *T*). Accordingly, the length of the CETN1-positive CC fragment is reduced to 78.5% in P25 (0.84 ± 0.13) and 56.3% (0.58 ± 0.14 μm) in 3m *Cetn2*$^{-/-}$;*Cetn3*$^{GT/GT}$ mice compared with WT controls (1.07 ± 0.18 at P25 and 1.03 ± 0.18 μm at 3m) (Fig. 6*U*). Further, CETN1 signal is stronger in both the P25 and 3m *Cetn2*$^{-/-}$;*Cetn3*$^{GT/GT}$ retina compared with controls (compare Fig. 6, *I* and *L*, with *O* and *R*); quantification of the fluorescence intensity revealed that the *Cetn2*$^{-/-}$;*Cetn3*$^{GT/GT}$ CETN1 signal is 1.25- and 1.67-fold of control at P25 and 3m, respectively (Fig. 6*V*). The photoreceptor CEP290 length is similar between *Cetn2*$^{-/-}$;*Cetn3*$^{GT/GT}$ and WT at P25 but slightly reduced in 3m *Cetn2*$^{-/-}$;*Cetn3*$^{GT/GT}$ mice (0.99 ± 0.16 μm) compared with WT (1.16 ± 0.21 μm) (Fig. 6*W*). These results indicate that in the absence of

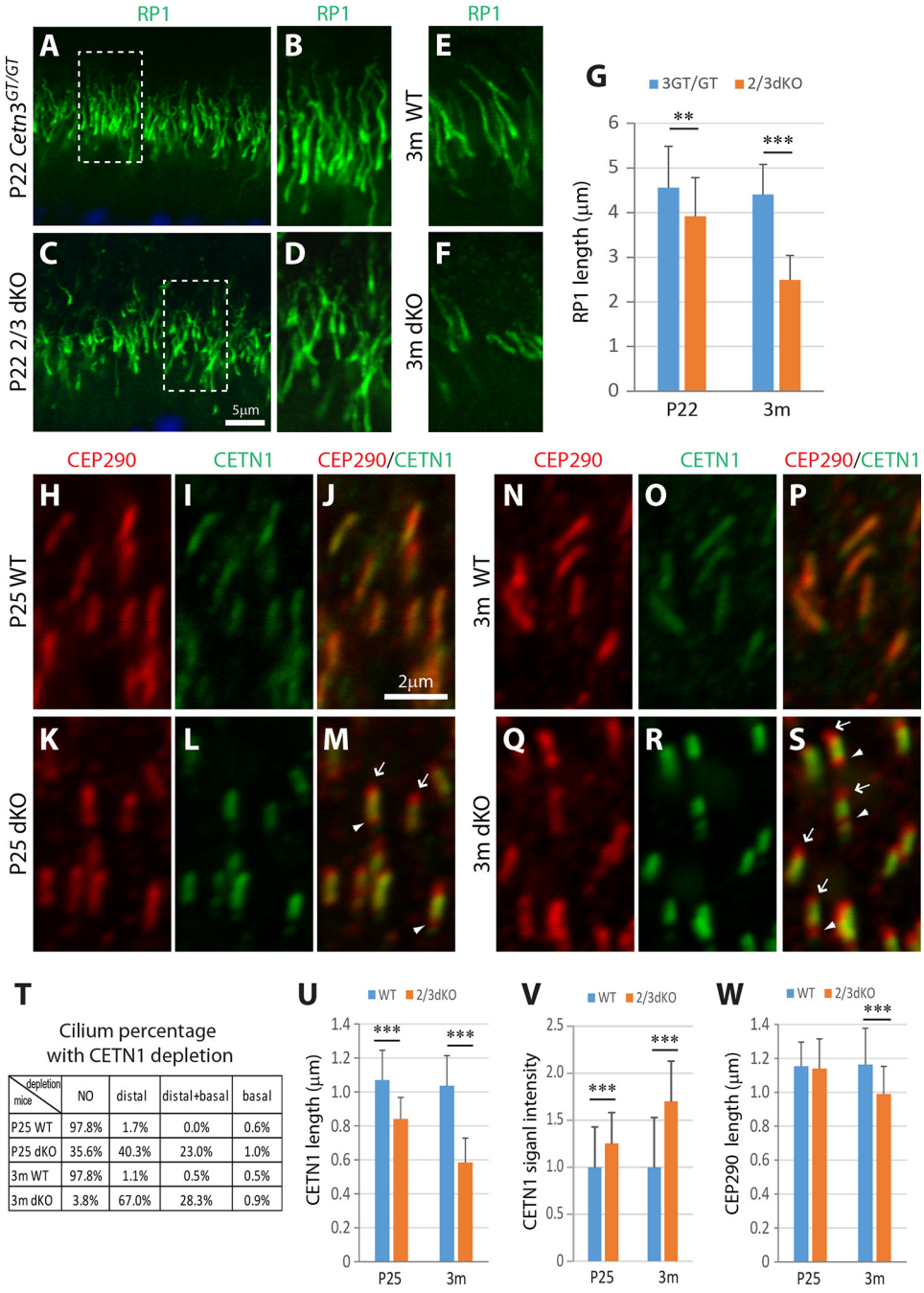

depletion / mice	NO	distal	distal+basal	basal
P25 WT	97.8%	1.7%	0.0%	0.6%
P25 dKO	35.6%	40.3%	23.0%	1.0%
3m WT	97.8%	1.1%	0.5%	0.5%
3m dKO	3.8%	67.0%	28.3%	0.9%

Figure 6. Reduced RP1-responsive axoneme length and centered CETN1 distribution in *Cetn2*$^{-/-}$;*Cetn3*$^{GT/GT}$ photoreceptor. *A–F*, RP1 immunostaining of retina sections of *Cetn3*$^{GT/GT}$ (*A*, *B*, and *E*) and *Cetn2*$^{-/-}$; *Cetn3*$^{GT/GT}$ (*C*, *D*, and *F*) at P22 (*A–D*) and 3 months (*E* and *F*). *B* and *D* are higher magnifications of the *boxed areas* in *A* and *C*, respectively. Note the reduction of RP1-positive axoneme length in *Cetn2*$^{-/-}$; *Cetn3*$^{GT/GT}$. *G*, quantification of RP-1 axoneme length. RP1 length is significantly reduced in *Cetn2*$^{-/-}$;*Cetn3*$^{GT/GT}$ photoreceptors compared with *Cetn3*$^{GT/GT}$ at both P22 and 3m. Shown are mean ± S.D., $n = 45–61$ for each group, one-way ANOVA, **, $p < 0.01$, ***, $p < 0.001$. *H–S*, CEP290 (*red*) and CETN1 (*green*) co-staining of WT (*H–J* and *N–P*) and *Cetn2*$^{-/-}$;*Cetn3*$^{GT/GT}$ (*K–M* and *Q–S*) at P25 (*H–M*) and 3 months (*N–S*). CEP290 and CETN1 overlap at the CC in WT, whereas in *Cetn2*$^{-/-}$;*Cetn3*$^{GT/GT}$, CETN1 is absent from both the distal and proximal CC (*arrows* and *arrowheads* in *M* and *S*) and concentrate to the mid-segment. *T*, CETN1 distribution at CC (percentage of normal), *i.e.* no end depletion (full-length overlap) between CEP290 and CETN1, distal end depletion, distal and proximal end depletion, and proximal end depletion in P25 and 3-month-old *Cetn2*$^{-/-}$;*Cetn3*$^{GT/GT}$ retinas. CC numbering 178 to 212 from each group, were analyzed. *U*, quantification of CETN1 length, which is significantly reduced in *Cetn2*$^{-/-}$;*Cetn3*$^{GT/GT}$ photoreceptors compared with WT at both time points. Shown are mean ± S.D.; $n = 48–73$ for each group, one-way ANOVA; **, $p < 0.01$, ***, $p < 0.001$. *V*, quantification of CETN1 fluorescence signal intensity. The signal is significantly increased in *Cetn2*$^{-/-}$;*Cetn3*$^{GT/GT}$ by 25 and 67% at P25 and 3m relative to the control (set as 1). Shown are mean ± S.D.; $n = 62–86$ for each group, one-way ANOVA; ***, $p < 0.001$. *W*, quantification of CEP290 length. RP1 length is comparable between P25 *Cetn2*$^{-/-}$;*Cetn3*$^{GT/GT}$ photoreceptors and WT but is significantly reduced in 3m *Cetn2*$^{-/-}$;*Cetn3*$^{GT/GT}$ photoreceptors compared with WT. Shown are mean ± S.D.; $n = 45–62$ for each group, one-way ANOVA; ***, $p < 0.001$. *Scale bars*: *A–F*, 5 μm; *H–O*, 2 μm.

both CETN2 and CETN3, CETN1 is gradually depleted from the CC distal and proximal ends and accumulates in the center, concurrent with a slight shortening of the *Cetn2*$^{-/-}$; *Cetn3*$^{GT/GT}$ CC.

Altered Cetn2$^{-/-}$;*Cetn3*$^{GT/GT}$ *ciliary microtubule acetylation*

Co-immunolabeling of P25 cryosections with anti-CEP290 and anti-acetylated α-tubulin (Ac-tubulin) identified WT CC (Fig. 7, *A–C*, *arrowheads*). The response concentrates at the

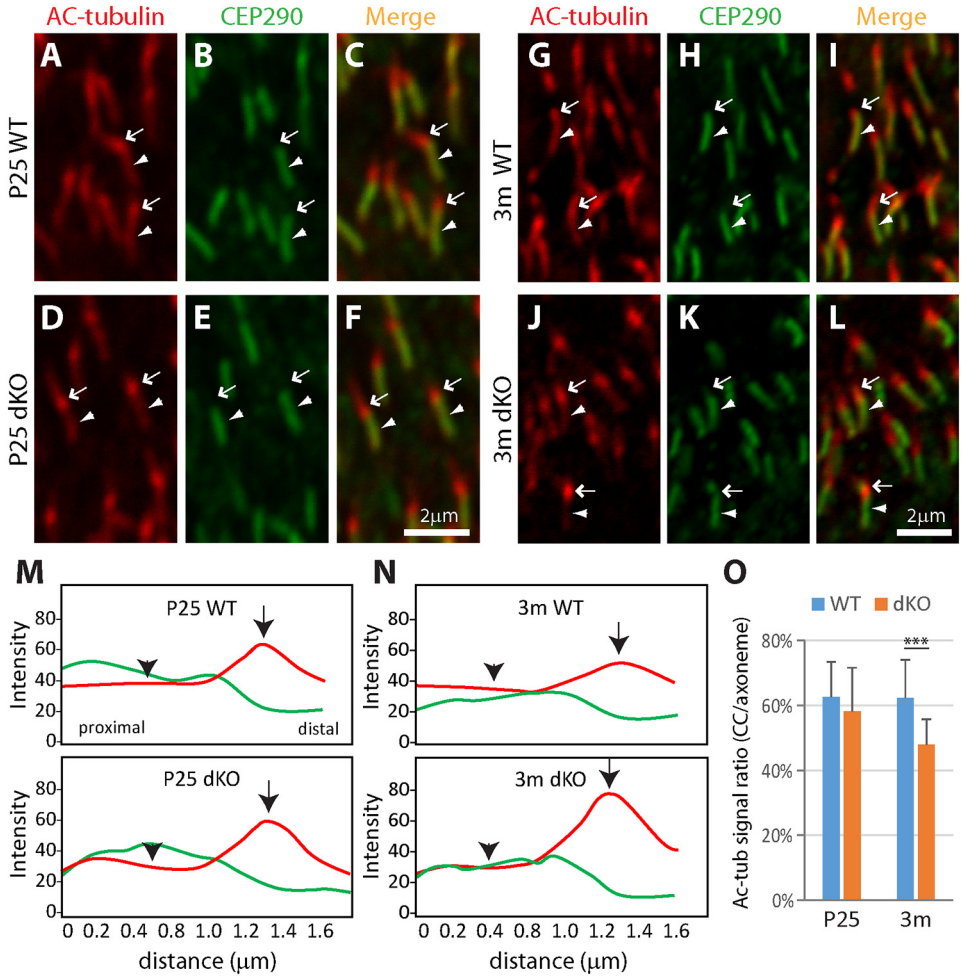

Figure 7. *Cetn2*$^{-/-}$;*Cetn3*$^{GT/GT}$ photoreceptors display tubulin hypoacetylation at CC and hyperacetylation at the proximal axoneme. *A–L*, Ac-tubulin (*red*) and CEP290 (*green*) co-staining of retina sections of WT (*A–C* and *G–I*) and *Cetn2*$^{-/-}$;*Cetn3*$^{GT/GT}$ (*D–F* and *J–L*) at P25 (*A–F*) and 3 months (*G–L*). Ac-tubulin colocalize with CEP290 at CC (*arrowheads*) but Ac-tubulin signal also extends into and peaks at the proximal axoneme (*arrows*) in P25 and 3-month-old WT photoreceptors. In P25 *Cetn2*$^{-/-}$;*Cetn3*$^{GT/GT}$, the pattern is similar. By 3 months, the Ac-tubulin signal at the CC is reduced (*arrowheads* in *J–L*), whereas the signal at the proximal axoneme is increased (*arrows* in *J–L*). *Scale bar*: 2 μm. *M* and *N*, representative Ac-tubulin (*red*) and CEP290 (*green*) signal profile along the CC–axoneme axis, starting from the CC proximal end of the WT (*top panels*) and *Cetn2*$^{-/-}$;*Cetn3*$^{GT/GT}$ (*bottom panels*) at P25 (*M*) and 3m (*N*). Note the peak of the Ac-tubulin signal at 1.2–1.4 μm with the sharp drop of CEP290 signal. *O*, quantification of Ac-tubulin signal ratio at CC *versus* proximal axoneme. The ratio was calculated by comparing the signal at the midpoint of the CC *versus* the signal peak of the OS axoneme base (measuring positions are marked by *arrowheads* and *arrows*). No difference was detected for the P25 samples, but at 3m the ratio is significantly lower in *Cetn2*$^{-/-}$;*Cetn3*$^{GT/GT}$ than in WT. Shown are mean ± S.D.; $n = 35–59$ for each group, one-way ANOVA; ***, $p < 0.001$.

proximal OS axoneme base (*arrows*) in both the P25 WT (Fig. 7, *A–C*) and *Cetn2*$^{-/-}$;*Cetn3*$^{GT/GT}$ photoreceptors (Fig. 7, *D–F*). At 3 months of age, the CEP290 and Ac-tubulin pattern of the WT was similar to that of P25 (Fig. 7, *G–I*), whereas in *Cetn2*$^{-/-}$;*Cetn3*$^{GT/GT}$ photoreceptors, the Ac-tubulin signal was concentrated primarily at the proximal axoneme (*arrows*) but greatly reduced from CEP290-positive CC (*arrowheads*, Fig. 7, *J–L*). We profiled the CEP290 and Ac-tubulin fluorescence along the CC and axoneme starting from the CC proximal end at the basal body (Fig. 7, *M* and *N*). The pattern was similar between P25 WT and *Cetn2*$^{-/-}$;*Cetn3*$^{GT/GT}$ photoreceptors with an Ac-tubulin signal peak and sharp CEP290 drop at the OS proximal axoneme (1.2–1.4 μm from the CC proximal end at the basal body) (Fig. 7*M*). By 3 months of age, the pattern was unchanged in the WT, but the Ac-tubulin signal was greatly increased at the *Cetn2*$^{-/-}$;*Cetn3*$^{GT/GT}$ OS axoneme base and reduced along the CC (Fig. 7*N*). The quantification results reveal comparable Ac-tubulin signal ratios (CC midpoint signal *versus* peak axoneme base signal) between P25 WT (62.7 ± 10.8%) and *Cetn2*$^{-/-}$;*Cetn3*$^{GT/GT}$ (58.2 ± 13.5%) (Fig. 7*O*). At 3 months, the ratio was significantly reduced in *Cetn2*$^{-/-}$;*Cetn3*$^{GT/GT}$ photoreceptors (47.9 ± 7.9%) compared with WT (62.2 ± 11.8%) (Fig. 7*O*), indicating a gradual deacetylation of CC microtubules but hyperacetylation of proximal OS axoneme microtubules.

Misaligned Cetn2$^{-/-}$;*Cetn3*$^{GT/GT}$ *OS discs and dilated CC/axonemes*

Ultrastructure of 2.5-month-old *Cetn3*$^{GT/GT}$ photoreceptors revealed normal, densely packed, vertically oriented rods with horizontally stacked OS discs (Fig. 8*A*). By contrast, the *Cetn2*$^{-/-}$;*Cetn3*$^{GT/GT}$ littermate OS structure was highly disorganized, as judged by overgrown and longitudinally aligned discs, membrane whorls, and expanded OS diameters (Fig. 8, *B–D*), resembling the phenotype seen in *Rp1*$^{-/-}$ or *Rp1* knockin mouse retinas (28, 29). There were also CC/axoneme structural abnormalities in the *Cetn2*$^{-/-}$;*Cetn3*$^{GT/GT}$ photore-

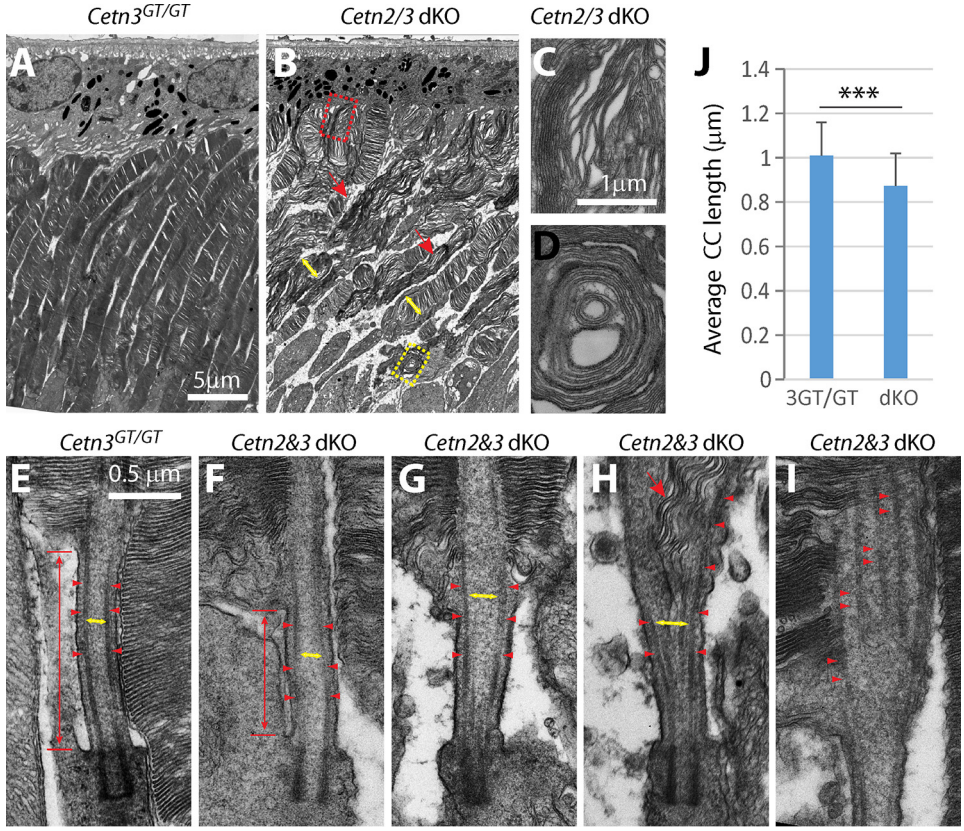

Figure 8. Distal CC expansion and OS disorganization of *Cetn2*$^{-/-}$;*Cetn3*$^{GT/GT}$ photoreceptors. *A* and *B*, representative electron micrographs of 2.5-month-old *Cetn3*$^{GT/GT}$ (*A*) and *Cetn2*$^{-/-}$;*Cetn3*$^{GT/GT}$ (*B*) retinas. Note the vertically aligned discs (*red arrows* and *red-boxed area* in *B*), membrane whorls (*red-boxed*), and increased OS diameters (*yellow double arrows* in *B*) in *Cetn2*$^{-/-}$;*Cetn3*$^{GT/GT}$. *C*, enlargement of *yellow-boxed area* in *B*. *D*, enlargement of *red-boxed area* in *B*. *E–I*, high magnification of *Cetn3*$^{GT/GT}$ (*E*) and *Cetn2*$^{-/-}$;*Cetn3*$^{GT/GT}$ (*F–I*) CC and proximal axoneme areas. Distal CC and proximal axonemes are expanded (*yellow double arrows*), ranging from minor (*F*) to intermediate (*G*) to severe (*H*) in *Cetn2*$^{-/-}$;*Cetn3*$^{GT/GT}$ compared with *Cetn3*$^{GT/GT}$. Note vertically aligned disc membranes in *H*. *I*, example of axoneme enlargement and microtubule spread at OS base. Four microtubules (*red arrowheads*) were visible in this plane, indicating disassembly of axonemal circular organization and microtubule flattening. CC length (referred to here as the length between the ciliary pocket and the first ciliary membrane evagination (*red double arrows*) is reduced in *Cetn2*$^{-/-}$;*Cetn3*$^{GT/GT}$. *J*, average CC length is significantly reduced in *Cetn2*$^{-/-}$;*Cetn3*$^{GT/GT}$ compared with *Cetn3*$^{GT/GT}$. Shown are mean ± S.D.; $n = 47$ (*Cetn3*$^{GT/GT}$) and 30 (*Cetn2*$^{-/-}$;*Cetn3*$^{GT/GT}$), one-way ANOVA; ***, $p < 0.001$.

ceptors. Control *Cetn3*$^{GT/GT}$ CC and axonemes had a normal diameter of ~250 nm (Fig. 8*E*). However, ~20–30% of the *Cetn2*$^{-/-}$;*Cetn3*$^{GT/GT}$ photoreceptors (depending on the mouse), of >60 CC that were examined from three samples, showed variable dilation at the distal CC (Fig. 8, *E–H*, *yellow double arrows*) and OS proximal axoneme (Fig. 8*I*, *red arrowheads*) not seen in WT controls. This phenotype ranged from a minor, slight expansion (Fig. 8*G*) to severe, extreme dilation with invasion of vertically aligned disc membranes (Fig. 8*H*) and loss of microtubule doublet integrity (not shown). Consistent with CEP290 immunolabeling (Fig. 6, *N–S* and *W*), the CC average length (Fig. 8, *E* and *F*, *red double arrows*) was slightly but significantly reduced in 2.5-month-old *Cetn2*$^{-/-}$;*Cetn3*$^{GT/GT}$ photoreceptors (0.87 ± 0.14 μm) compared with *Cetn3*$^{GT/GT}$ controls (1.01 ± 0.15 μm) (Fig. 8*J*). These observations suggest that CETN2 and CETN3 are required for CC length and structural maintenance, which direct photoreceptor OS disc assembly.

Gradual depletion of SPATA7 from Cetn2$^{-/-}$;*Cetn3*$^{GT/GT}$ *CC*

The photoreceptor-specific distal CC is maintained by SPATA7 (spermatogenesis-associated protein 7), knockout of which in the mouse leads to radial expansion of the distal CC microtubular array (26). To determine whether the observed CC/axonemal dilation of *Cetn2*$^{-/-}$;*Cetn3*$^{GT/GT}$ photoreceptors involved SPATA7, we investigated SPATA7 expression at P25, 2m, and 3m. Colocalization of SPATA7 and Ac-tubulin at P25 revealed that SPATA7 labeled the CC of *Cetn2*$^{-/-}$;*Cetn3*$^{GT/GT}$ and control photoreceptors comparably (Fig. 9, *A–J*, *green*). At 2m, SPATA7 is partially depleted, starting from the mid-segment (Fig. 9, *K–O*), and by 3m SPATA7 is virtually nondetectable along the entire *Cetn2*$^{-/-}$;*Cetn3*$^{GT/GT}$ CC (Fig. 9, *P–T*). Thus, distal CC dilation of *Cetn2*$^{-/-}$;*Cetn3*$^{GT/GT}$ photoreceptors correlates with SPATA7 depletion. SPATA7 forms a complex with RPGRIP (RPGR-interacting protein) and RPGR (retinitis pigmentosa GTPase regulator) proteins at CC (26). However, whereas both RPGR (Fig. 10, *A–F*) and RPGRIP (Fig. 10, *G–L*) are still expressed in the CC of 3-month-old *Cetn2*$^{-/-}$;*Cetn3*$^{GT/GT}$ mice, RPGRIP shows a slight depletion from the mid-segment relative to controls (Fig. 10, *J–L*, *arrows*).

As misaligned OS membrane discs feature prominently in the photoreceptors of the *retina degeneration slow* (*rds*, peripherin 2) heterozygous mouse (30), the prominin 1 (R373C) transgenic mouse (31), and the *C8orf37*$^{-/-}$ mouse (32), we tested these protein levels and localizations in the *Cetn2*$^{-/-}$;*Cetn3*$^{GT/GT}$ retina. A retina lysate immunoblot showed that the peripherin 2 level is similar in *Cetn2*$^{-/-}$;*Cetn3*$^{GT/GT}$ and

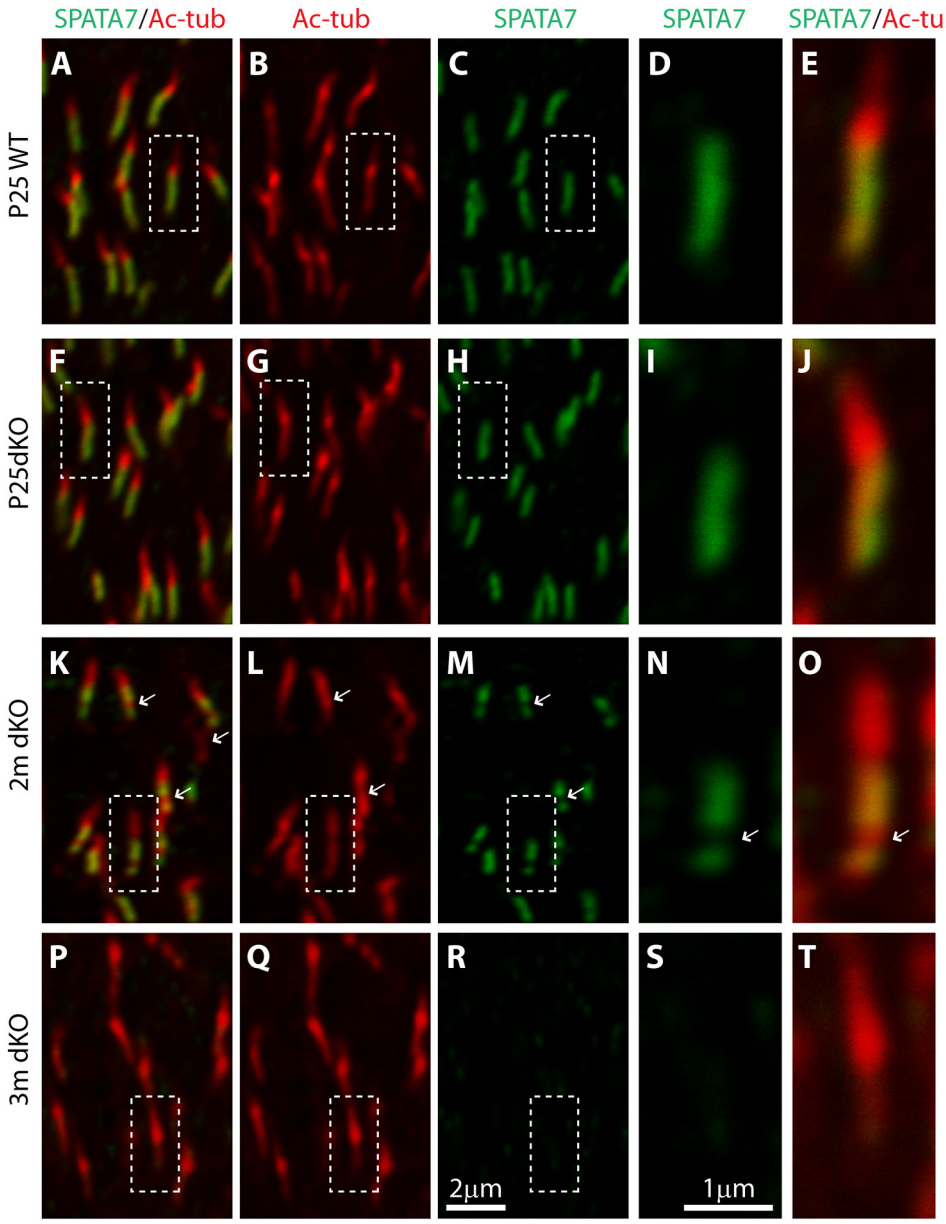

Figure 9. SPATA7 is gradually depleted from CC of *Cetn2*$^{-/-}$;*Cetn3*$^{GT/GT}$ photoreceptors. *A–E*, SPATA7 (*green*) and Ac-tubulin (*red*) co-staining of P25 WT retina. *D* and *E* are higher magnifications of the *boxed areas* in *C* and *A*, respectively. SPAT7 is located specifically at the CC. *F–T*, SPATA7 (*green*) and Ac-tubulin (*red*) co-staining of *Cetn2*$^{-/-}$;*Cetn3*$^{GT/GT}$ retina at P25 (*F–J*), 2m (*K–O*), and 3m (*P–T*). *I*, *J*, *N*, *O*, *S*, and *T* are higher magnifications of *boxed areas* in *H*, *F*, *M*, *K*, *R*, and *P*, respectively. There is no depletion at P25. By 2m, SPATA7 is partially depleted from the mid-segment of CC (*arrows* in *K–O*), and by 3m, SPATA7 is almost completely depleted along the full-length CC. *Scale bars*: *A–C*, *F–H*, *K–M*, and *P–R*, 2 μm; *D*, *E*, *I*, *J*, *N*, *O*, *S*, and *T*, 1 μm.

Cetn3$^{GT/GT}$ retinas (Fig. 11*A*). Although altered ciliary tubulin acetylation occurs in *Cetn2*$^{-/-}$;*Cetn3*$^{GT/GT}$, we did not observe any significant Ac-α-tubulin level change (Fig. 11*A*). Distributions of peripherin 2 to the OS (Fig. 11, *B* and *C*) and prominin 1 to the OS base (Fig. 11, *D* and *E*) were preserved in *Cetn2*$^{-/-}$;*Cetn3*$^{GT/GT}$ as in the *Cetn3*$^{GT/GT}$ control retina. In addition, the intraflagellar transport protein IFT88 correctly localized to the basal body and OS axoneme base as two pools (basal body and proximal OS) in both *Cetn2*$^{-/-}$;*Cetn3*$^{GT/GT}$ and control photoreceptors (Fig. 11, *F* and *G*) and as reported (33).

Discussion

We generated *Cetn3*$^{GT/GT}$ and *Cetn2*$^{-/-}$;*Cetn3*$^{GT/GT}$ mouse lines to investigate the function of CETN2 and CETN3 in photoreceptors. We had observed previously the absence of a retinal phenotype in *Cetn1*$^{-/-}$ and *Cetn2*$^{-/-}$ mice (22, 23), suggesting centrin redundancy. Here, we found that 1-year-old *Cetn3*$^{GT/GT}$ single knockouts exhibited completely normal retina morphology and function. However, *Cetn2*$^{-/-}$;*Cetn3*$^{GT/GT}$ mice revealed progressive retina degeneration starting at 1 month of age, which was nearly complete in the dorsal retina 1 year later. Our main results were as follows: (i) *Cetn2*$^{+/-}$;*Cetn3*$^{GT/GT}$ mice display reduced scotopic a- and photopic b-waves, signaling haploinsufficiency (one allele of *Cetn2* is insufficient to establish the WT phenotype); (ii) *Cetn2*$^{-/-}$;*Cetn3*$^{GT/GT}$ mice are born in a non-Mendelian ratio, suggesting loss of embryos during embryonic development; (iii) *Cetn2*$^{-/-}$;*Cetn3*$^{GT/GT}$ photoreceptor CC are shortened and dilated dis-

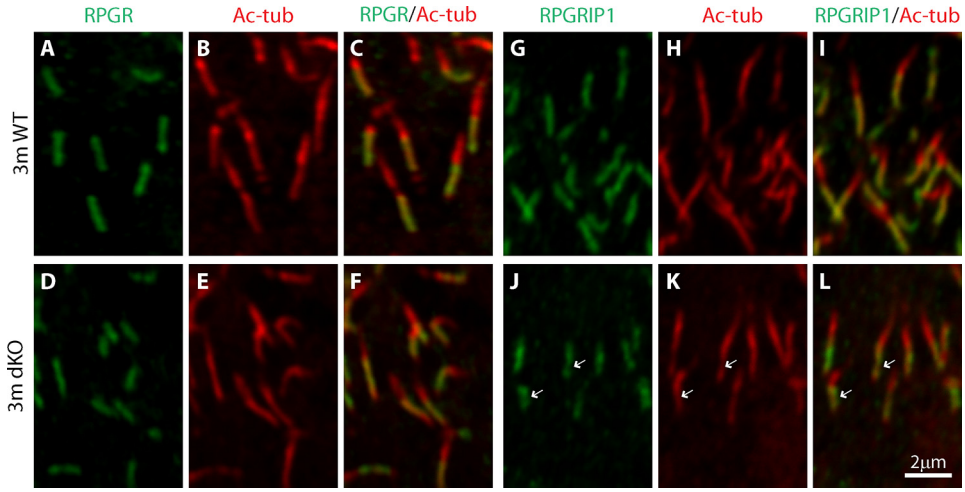

Figure 10. RPGR and RPGRIP correctly locate to the CC in 3m *Cetn2*$^{-/-}$;*Cetn3*$^{GT/GT}$ photoreceptors. *A–F*, RPGR (*green*) and Ac-tubulin (*red*) co-staining of 3m WT (*A–C*) and *Cetn2*$^{-/-}$;*Cetn3*$^{GT/GT}$ (*D–F*) retina. *G–L*, RPGRIP (*green*) and Ac-tubulin (*red*) co-staining of 3m WT (*G–I*) and *Cetn2*$^{-/-}$;*Cetn3*$^{GT/GT}$ (*J–L*) retina. There is no depletion of RPGR, whereas RPGRIP is slightly reduced at some mid-segment CC (*arrows*, *J–L*) of *Cetn2*$^{-/-}$;*Cetn3*$^{GT/GT}$. *Scale bar*: 2 μm.

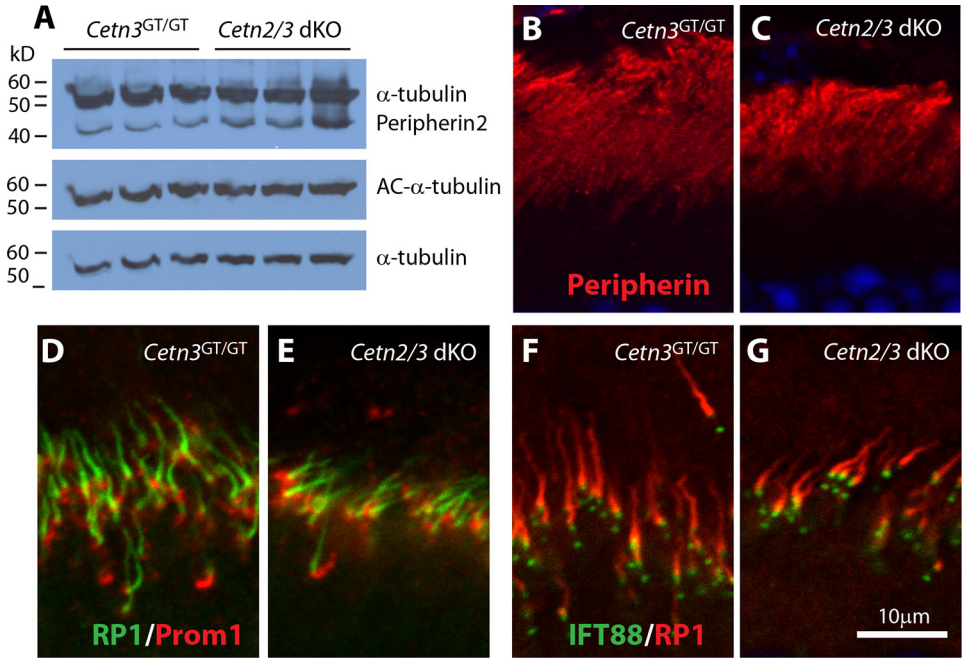

Figure 11. Peripherin 2, prominin 1, and IFT88 are located correctly in 3m *Cetn2*$^{-/-}$;*Cetn3*$^{GT/GT}$ photoreceptors. *A*, immunoblot of peripherin 2 and Ac-tubulin levels associated with retina lysate harvested from 1-month-old *Cetn3*$^{GT/GT}$ and *Cetn2*$^{-/-}$;*Cetn3*$^{GT/GT}$ (Cetn2/3 dKO) mice; α-tubulin was used as loading control. *B–G*, peripherin 2 staining (*B* and *C*), RP1 (*green*) and prominin 1 (*red*) co-staining (*D* and *E*), and RP1 (*red*) and IFT88 (*green*) co-staining of 3 month-old *Cetn3*$^{GT/GT}$ (*B*, *D*, and *F*) and *Cetn2*$^{-/-}$;*Cetn3*$^{GT/GT}$ (*C*, *E*, and *G*) retina. The pattern of every protein is comparable between *Cetn2*$^{-/-}$;*Cetn3*$^{GT/GT}$ and *Cetn3*$^{GT/GT}$. *Scale bar*: 10 μm.

tally; and (iv) SPATA7 depletes and CETN1 concentrates in the mid-segment of the mutant CC (Fig. 12). The results demonstrate that CETN2 and CETN3 together stabilize the photoreceptor distal CC and proximal OS axoneme by interacting with the protein complex of which SPATA7 is a member.

Unlike their orthologs in lower eukaryotes (34–36), the requirement for vertebrate centrins in centriole duplication (9, 11–14) or ciliogenesis (15, 23) is still controversial with inconsistent results among different studies. Although we have not directly assessed centriole duplication, the lack of detectable phenotype in *Cetn3*$^{GT/GT}$ mice indicates that CETN3 is dispensable for centriole duplication in mouse, in contrast to a previous study with *Xenopus* embryos in which ectopic recombinant human CETN3 protein inhibits centriole duplication and blastomere cleavage (14). As *Cetn2*$^{-/-}$ pups are born slightly below a Mendelian ratio (Table 1), CETN2 is probably required for centriole duplication in a small percentage of mouse embryos (23). However, the severely reduced *Cetn2*$^{-/-}$;*Cetn3*$^{GT/GT}$ pup ratio (29.2% *versus* theoretical 50% (Table 1)) indicates that normal mouse embryo development requires both CETN2 and CETN3, implying that CETN2 and CETN3 are both required for centriole duplication and mitosis during embryonic development. Why some embryos can escape CETN2/CETN3 deficiency but others cannot and why only selected tissues show ciliopathy in *Cetn2*$^{-/-}$;*Cetn3*$^{GT/GT}$ mice, despite the ubiquitous expression of CETN2 and CETN3, is unknown. Incom-

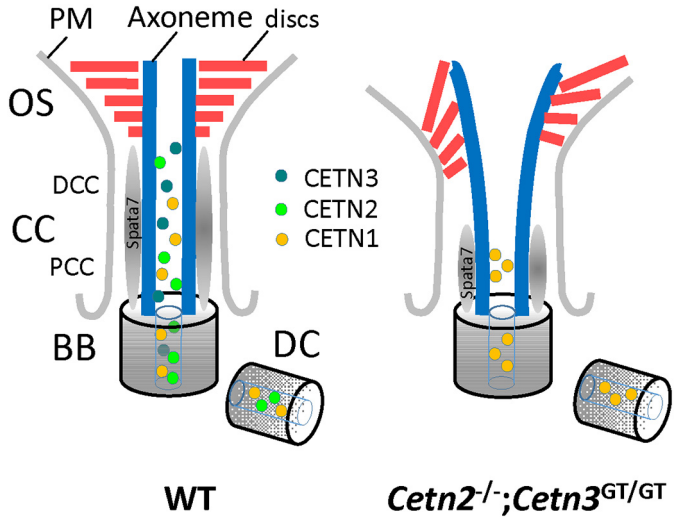

Figure 12. Model of CETN2 and CETN3 function in mouse photoreceptors. In WT photoreceptors, CETN1–3 are localized to the CC and the centriole lumen formed by the inner microtubule wall. SPATA7 is located outside along the outer CC microtubule wall. The axoneme (diameter of ~250 nm) extends into the OS where discs are formed. In *Cetn2*$^{-/-}$;*Cetn3*$^{GT/GT}$ photoreceptors, CETN1 accumulates at the CC center and SPATA7 is gradually depleted from the CC outside wall. As a consequence, distal CC and basal OS axonemes are destabilized, the microtubule structure disintegrates, and OS discs misalign; *BB*, basal body; *DC*, daughter centriole.

plete penetrance is often observed in ciliopathy, caused by basal body gene mutations (37).

Given centrin localization in the basal body and connecting cilium lumen, photoreceptors are an excellent system to use for studying the roles of CETN2 and CETN3 in postmitotic neurons. Our results show that CETN2 and CETN3 are together required for photoreceptor survival after maturation. In the absence of CETN2 and CETN3, CC and axonemes display molecular and structural changes, including reduction of the RP1 decoration of proximal OS axonemes (Fig. 6), CETN1 accumulating at the center of the CC but depleted from the distal and proximal ends (Fig. 6), microtubule hypoacetylation at the CC but hyperacetylation at the proximal OS axoneme (Fig. 7), SPATA7 depletion from the *Cetn2*$^{-/-}$;*Cetn3*$^{GT/GT}$ CC (Fig. 9), CC shortening (Figs. 6 and 8), and distal CC and proximal OS axoneme expansion (Figs. 8 and 12). RP1 is a photoreceptor-specific axoneme- and microtubule-binding protein. RP1 knockout, or knockin of a mutant form, causes progressive retina degeneration and disc morphogenesis defects (28, 29). Notably, *Cetn2*$^{-/-}$;*Cetn3*$^{GT/GT}$ mice showed OS malformation and disorganization very similar to that seen in RP1 mutants, *i.e.* vertically misaligned discs, membrane whorls, and disc expansion (Fig. 8), which could occur in RP1 mutants as early as P7 when rod OS discs first assemble (28, 29). Apart from OS disc orientation, RP1 is also important in controlling the length and stability of the photoreceptor axoneme (27). Despite these similarities, noticeable phenotypic differences do exist in *Cetn2*$^{-/-}$;*Cetn3*$^{GT/GT}$ mice relative to RP1 mutants. First, the photoreceptor degeneration is slower in the *Cetn2*$^{-/-}$;*Cetn3*$^{GT/GT}$ retina. RP1 retina degeneration is nearly complete by 10 months (28, 29), but in 13-month-old *Cetn2*$^{-/-}$;*Cetn3*$^{GT/GT}$ mice, the ventral retina still has 4–5 rows of ONL nuclei (Fig. 3*A*). Second, faster degeneration of the dorsal *versus* the ventral retina is unique to *Cetn2*$^{-/-}$;*Cetn3*$^{GT/GT}$ mice (Fig. 3*A*). Third, dilation of the CC and axoneme (Fig. 8) and extreme swelling of the *Cetn2*$^{-/-}$;*Cetn3*$^{GT/GT}$ cone OS (Fig. 5, *C–E*) have not been reported for RP1 mutants.

Ciliary tubulin hypoacetylation, proximal OS axoneme tubulin hyperacetylation, and CETN1 depletion from the CC distal ends in *Cetn2*$^{-/-}$;*Cetn3*$^{GT/GT}$ photoreceptors are intriguing observations. Tubulin acetylation is a hallmark of long-lived, stable microtubules. Mice lacking αTAT1 (α-tubulin acetyltransferase 1), the enzyme predominantly responsible for α-tubulin acetylation *in vivo*, are viable and display no overt phenotypes except for the deformation of the dentate gyrus (38). Whether a TAT1-deficient mouse has a retina phenotype has not been reported. Recently, it was found that intraluminal tubulin acetylation protects microtubules from mechanical breakage by weakening the lateral interaction of protofilaments and enhancing microtubule flexibility (39, 40). As microtubule bending occurs in response to the mechanical force generated by microtubule motor movement (41) and actomyosin contractility (42, 43), we predict that a consequence of CC hypoacetylation would be reduced resistance to microtubule bending and increased probability of breakage at CC. This notion is supported by the observation of the expansion/break of the distal CC and proximal axoneme (Fig. 8 and not shown). How centrins regulate tubulin acetylation is largely unknown. Centrins are localized within the CC lumen along the microtubule surface (24, 25), but α-tubulin acetylation and deacetylation occur on Lys-40, located at the microtubule intraluminal side. Thus, centrins may indirectly regulate Lys-40 acetylation by αTAT1 (44) or deacetylation by HDAC6 (histone deacetylase 6) (45), and one possibility is that centrins regulate the entry of αTAT1 or HDAC6 into the microtubule lumen.

The photoreceptor CC has long been considered analogous to the TZ of the prototypic primary cilium, but a recent study shows that the photoreceptor distal CC (DCC) is uniquely maintained by a retina-specific ciliopathy protein, SPATA7 (26). Common TZ proteins (such as NPHP1, NPHP4, NPHP6, AHI1, RPGR, and RPGRIP) are lost specifically in *Spata7*$^{-/-}$ DCC but not the proximal *Spata7*$^{-/-}$ CC of mouse photoreceptors, which collectively cause microtubule destabilization and axoneme radial expansion (26). In the *Cetn2*$^{-/-}$;*Cetn3*$^{GT/GT}$ mouse, SPATA7 is gradually depleted from the CC (Fig. 9), which provides a mechanistic explanation for the DCC/axoneme dilation phenotype. Interestingly, although SPATA7 is nearly completely depleted from the 3m *Cetn2*$^{-/-}$;*Cetn3*$^{GT/GT}$ photoreceptor CC, RPGR, RPGRIP (Fig. 10), and NPHP6 proteins (Figs. 6 and 7) are positioned normally (RPGR and NPHP6) or affected minimally (RPGRIP). These observations suggest that loss of transition zone proteins, including RPGR and RPGRIP, may not fully account for the DCC microtubule phenotype seen in *Spata7*$^{-/-}$ mouse. Alternatively, as a microtubule-associated protein (46), SPATA7 may stabilize microtubules directly. Notably, CETN2 specifically is lost from the DCC of *Spata7*$^{-/-}$ photoreceptors (26). DCC dilation is also observed in the *Fam161a* knockout mouse, a model of human RP28 characterized by CETN3 exclusion from the CC (47). We observed that CETN1 is depleted from the DCC and, to a lesser extent, from the proximal CC in *Cetn2*$^{-/-}$;

Cetn3$^{GT/GT}$ photoreceptors (Fig. 6). Centrins are not only perfect molecular markers for CC but also actively participate in maintaining connecting cilium and proximal axoneme structural stability. How CETN2 and CETN3 interact specifically and regulate SPATA7 localization warrants further investigation.

In summary, CETN2 and CETN3 have redundant functions *in vivo*. Our *Cetn2*$^{-/-}$;*Cetn3* $^{GT/GT}$ mouse is a valuable model for studying centrin function in centriole duplication and ciliogenesis. CETN2 and CETN3 are both required for photoreceptor survival by regulating SPATA7 CC localization, DCC/axoneme microtubule stability, and OS disc orientation (see model in Fig. 12).

Experimental procedures

Animals

Mouse procedures were approved by the University of Utah Institutional Animal Care and Use Committee (IACUC) and were conducted in compliance with the NIH Guide for Care and Use of Laboratory Animals.

Generation of *Cetn3*$^{GT/GT}$ and *Cetn3*$^{-/-}$ mouse

Cetn3 embryonic stem (ES) cells (clones EPD0630_2_E12 and_ EPD0630_2_B09) on a C57BL/6N genetic background, JM8A3.N1 subline) and containing a gene trap (GT) in intron 2, were acquired from EUCOMM (Helmholtz Zentrum, Munich, Germany). ES cell blastocyst injection and generation of chimera and heterozygous (GT/+) mice were performed at the University of Utah Transgenic Gene-targeting Mouse Core Facility. The *rd8* mutation (48) was removed by crossing our *Cetn3*$^{GT/+}$ animals with C57BL/J WT mice. We mated *Cetn3*$^{GT/GT}$ with flippase (*Flp*) mice (C57BL/6 background) to generate animals with a floxed allele (*Cetn3*$^{fl/+}$) (Fig. 1*A*). Exon 3 was deleted by crossing *Cetn3*$^{fl/fl}$ with CMV-Cre mice (C57BL/6 background) to generate *Cetn3*$^{+/-}$ and *Cetn3*$^{-/-}$ mice. Mice were maintained under 12-h cyclic dark/light conditions. ES cell and mouse tail genomic DNA was extracted using a standard protocol (49). Routine PCR genotyping was performed using genomic DNA prepared with HotSHOT (50) as the template, along with genotyping primers and other primers (see below and listed in Table 2).

Electroretinography

ERG was performed on 8-month-old *Cetn3*$^{GT/GT}$, *Cetn3*$^{GT/+}$, and WT controls and on 1- and 3-month-old *Cetn2*$^{-/-}$;*Cetn3*$^{GT/GT}$, *Cetn2*$^{+/-}$;*Cetn3*$^{GT/GT}$, and *Cetn3*$^{GT/GT}$ animals (n = 5/group) using a UTAS E-3000 universal electrophysiological system (LKC Technologies) as described (23). Briefly, mice were dark-adapted overnight, anesthetized by intraperitoneal injection of ketamine (100 μg/g body weight) and xylazine (10 μg/g body weight) in 0.1 M PBS, and positioned on a recording platform with body temperature maintained at 37 ± 0.5 °C. After pupils were dilated with 1% tropicamide solution (Bausch & Lomb Inc., Tampa, FL), ERG responses were recorded from 5 mice of each genotype/time point. For scotopic ERG, mice were tested at intensities ranging from −1.63 log cd s/m^2 to 2.38 log cd s/m^2. For photopic ERG, a rod-saturating background light of 1.3979 log cd s/m^2 was applied for 20 min before and during recording at −0.01 log cd s/m^2 to 1.86 log cd s/m^2. Bacitracin ophthalmic ointment (Perrigo, Minneapolis, MN) was routinely applied to the eye to prevent infection after ERG testing, and animals were kept on a heating pad until fully recovered before being returned to cages. Peak amplitudes for both a- and b-waves were used for analysis using a one-way ANOVA test.

Table 2
PCR primers used for genotyping

Primer name	Sequences
5′-Arm-forward	CTCAAGGTCTGAACTCTAATCACAC
5′-Arm-reverse	CACAACGGGTTCTTCTGTTAGTCC
3′-Arm-forward	ACCTCCCCCTGAACCTGAAAC
3′-Arm-reverse	GCACTTATCATTCTATCATTAACAGTGAAC
1st FRT-forward	CTCCACTACCTCCACTTGTTACTG
1st FRT-reverse	CACAACGGGTTCTTCTGTTAGTCC
2nd LoxP-forward	GCGTCGAGAAGTTCCTATTCC
2nd LoxP-reverse	GGCTAGACAAAAGCATAAAAGCAGG
3rd LoxP-forward	GAAGTTGGTATGTACTTAGTCGCC
3rd LoxP-reverse	CACAGCGCACAGCAGTCTTC
Floxed allele-F1	CTCCACTACCTCCACTTGTTACTG
Floxed allele-F2	GCGTCGAGAAGTTCCTATTCC
Floxed allele-reverse	GGCTAGACAAAAGCATAAAAGCAGG
KO allele-F1	CTCCACTACCTCCACTTGTTACTG
KO allele-F2	GAAGTTGGTATGTACTTAGTCGCC
KO allele-reverse	CACAGCGCACAGCAGTCTTC

Measurement of ONL thickness and OS length

Average ONL thickness and OS length were measured based on DAPI and anti-GC1 antibody fluorescence as described (51). Eyes from WT or knockout mice were removed, marked on the nasal side for orientation, cut into cryosections, and labeled with DAPI and anti-GC1 mAb. The outer nuclear layer and outer segment layers were defined by DAPI and GC1, respectively. Three measurements of the outer nuclear layer and outer segment layers were taken every 200 μm from the optic nerve and averaged. The optic nerve was defined as 0 μm.

Confocal immunolocalization

The incubation of cryosections with antibodies and confocal imaging was performed as described (52) with minor modification. For photoreceptor OS proteins, eyecups were fixed by immersion in ice-cold 4% paraformaldehyde, cryoprotected in 30% sucrose, and embedded in OCT compound. Sections (12-μm thick) were cut using a Microm cryostat and mounted on charged Superfrost® Plus slides (Fisher). For antibodies against ciliary markers CETN3, CETN1, Ac-tubulin, and CEP290 and against SPATA7, RPGR, and RPGRIP, eyecups were embedded directly in OCT compound and cut into 12-μm sections. Sections were fixed in −20 °C methanol for 20 min or 4% paraformaldehyde for 5 min before immunolabeling. For RPGR and RPGRIP, the sections were further treated with 0.5% SDS for 5 min after paraformaldehyde fixation. Sections were washed in 0.1 M PBS, blocked using 10% normal goat serum or 2% BSA and 0.3% Triton X-100 in PBS, and incubated with primary antibodies at 4 °C overnight. After the PBS washes, signals were detected using Cy3- or Alexa 488 – conjugated goat anti-rabbit/mouse and/or donkey anti-goat/rabbit/mouse secondary antibody (Jackson ImmunoResearch) and contrasted with 1 μl/ml DAPI (Invitrogen). The primary antibodies and their sources, including references and dilutions, were: preab-

sorbed rabbit polyclonal anti-CETN3 and anti-CETN1(1:500, kindly provided by Dr. Uwe Wolfrum, University of Mainz, Germany) (24, 25); cone arrestin (mCAR 1:500) (53); CEP290 (1:300, Dr. Anand Swaroop, National Institutes of Health, NEI) (54); SPATA7 (1:100, Dr. Rui Chen, Baylor College of Medicine, Houston) (46); RPGR (55) and RPGRIP (56) (both at 1:500, Dr. Tiansen Li, NEI); mouse monoclonal anti-rhodopsin (1D4, 1:1000) (57); ROM-1 (1D5, 1:25) (58) and peripherin 2 (2B6, 1:25) (59) (Dr. Robert Molday, University of British Columbia-Vancouver); GC1 (IS4, 1:1000, Dr. Kris Palczewski, UC Irvine, CA) (60); chicken anti-RP1 (1:1000, Dr. Eric Pierce, Harvard University) (61); rat anti-CEP290 (1:300, Dr. Anand Swaroop, NEI) (62); anti-prominin 1 (mAb 13A4, 1:1000, Dr Wieland Huttner, Max Planck Institute, Dresden, Germany) (63); and goat anti-IFT88 (1:500, Dr. Greg Pazour, University of Massachusetts Medical School) (64). Commercial primary antibodies used included rabbit polyclonal anti-ML- and S-opsins (Chemicon, 1: 1500); PDE6 (MOE, Cytosignal, 1:1500); mouse monoclonal cyclic nucleotide-gated channel α1 and α3 (CNGA1/A3) (1: 1000, NeuroMab, UC Davis); and acetylated α-tubulin (T5451, Sigma, 1:1000). All of these were validated by Western blotting and/or immunostaining by the manufacturers and widely used in the literature. Images were captured using a Zeiss LSM-800 confocal microscope, with some images adjusted for brightness and contrast using Adobe Photoshop CS3.

Measurement of CC length and CETN1 signal intensity

Confocal RGB (red, green, and blue) images were split into 8-bit single-channel images using ImageJ 1.52a. For measuring the ciliary length defined by CEP290 and CETN1 co-labeling, CC were outlined with an integrated Find Edges plugin (Process-Find Edges) and then thresholded (Image-Adjust-Threshold) to generate binary images with background removed but the outlines of the majority of the CC kept. The same settings (default mode; low threshold between 10 and 40, high threshold 255) were applied to both the control and the experimental groups. Individual long axes (curved or straight) of the CC were labeled using a Freehand line-drawing tool; ROI manager (Analyze-Tools-ROI Manager) was added, and the length was measured. For analyzing CC CETN1 fluorescence intensity, green channel images were first treated with a median mode filter (radius, 5 pixels) to reduce the background and then thresholded (default mode; low threshold 20, high threshold 255) to generate the binary images. Individual ciliary regions were outlined using the Freehand line tool and added to the ROI Manager. The integrated intensity of ciliary region was measured and exported to Microsoft Excel.

Retina protein extraction and immunoblot

Retinas were homogenized in radioimmune precipitation assay buffer (10 mM Tris-Cl, pH 8.0, 140 mM NaCl, 1% Triton X-100, 0.1% sodium deoxycholate, 0.1% SDS, 1 mM EDTA, and 1 mM phenylmethylsulfonyl fluoride) and centrifuged (13,000 × *g* at 4 °C for 20 min), and supernatants were collected. Protein samples were separated by 10–12% SDS-PAGE, transferred to a polyvinylidene difluoride membrane, and probed with primary antibodies (anti-peripherin 2, Ac-α-tubulin, and α-tubulin) followed by horseradish peroxidase–conjugated secondary antibody. Antigens were visualized using an ECL Plus kit (Pierce).

Electron microscopy

2.5-Month-old *Cetn3*$^{GT/GT}$ and *Cetn2*$^{-/-}$;*Cetn3*$^{GT/GT}$ retinas (n = 3/group) were immersion-fixed for 2 h in fixative (2% glutaraldehyde and 1% paraformaldehyde in 0.1 M sodium cacodylate buffer, pH 7.4) at 4 °C, postfixed for 1 h in 1% osmium tetroxide, and stained *en bloc* with uranyl acetate. The washed specimens were dehydrated through an ascending series of methanol, dried in propylene oxide, and infiltrated overnight with a resin/propylene oxide (1:1) mixture followed by 100% Epon resin for 2 days. Specimens were embedded in plastic, and the plastic was cured by incubation in a 60 °C oven for 2 days. Blocks were trimmed, and 1-μm-thick sections were cut to orient photoreceptors near the optic nerve. Ultrathin sections at 60 nm were cut, placed onto slot grids with carbon-coated Formvar film (EMS, Hatfield, PA), post-stained with uranyl acetate followed by lead citrate, and finally examined using a JOEL electron microscope at 75 kV. CC length, defined as the distance between the ciliary pocket base and the first ciliary membrane evagination, was measured. The measurement was repeated by a person blinded to animal genotypes to verify the results.

Statistics

Data are presented as mean ± S.D., where n represents the number of mice (ERG and retina measurement) or number of photoreceptors (CC staining analysis). Statistical comparisons (significance level set at $p < 0.05$) were performed using one-way ANOVA for all experimental data.

Author contributions—G. Y., J. M. F., and W. B. conceptualization; G. Y. data curation; G. Y., J. M. F., and W. B. formal analysis; G. Y. and W. B. investigation; G. Y. and J. M. F. methodology; J. M. F. validation; W. B. funding acquisition; W. B. project administration.

Acknowledgments—We thank the following investigators for providing antibodies: Dr. Uwe Wolfrum (University of Mainz, Germany) for CETN3 and CETN1 antibodies; Dr. Robert Molday (University of British Columbia-Vancouver) for rhodopsin (1D4), Rom1 (1D5) and peripherin 2 (2B6) antibodies; Dr. Kris Palczewski (UC-Irvine) for GC1 (IS4) antibody; Dr. Eric Pierce (Harvard) for RP1 antibody; Dr. Anand Swaroop (National Institutes of Health, NEI) for CEP290 antibody; Dr. Rui Chen (Baylor College of Medicine) for SPATA7 antibody; Dr. Tiansen Li (NEI) for RPGR and RPGRPI antibodies; Dr. Wieland Huttner (MPI Dresden/Germany) for prominin 1 (13A4) antibody; and Dr. Greg Pazour (University of Massachusetts Medical School) for IFT88 antibody.

References

1. Hartman, H., and Fedorov, A. (2002) The origin of the eukaryotic cell: A genomic investigation. *Proc. Natl. Acad. Sci. U.S.A.* **99,** 1420–1425 CrossRef Medline
2. Thompson, J. R., Ryan, Z. C., Salisbury, J. L., and Kumar, R. (2006) The structure of the human centrin 2-xeroderma pigmentosum group C protein complex. *J. Biol. Chem.* **281,** 18746–18752 CrossRef Medline

3. Baron, A. T., Greenwood, T. M., Bazinet, C. W., and Salisbury, J. L. (1992) Centrin is a component of the pericentriolar lattice. *Biol. Cell* **76,** 383–388 CrossRef Medline
4. Baron, A. T., and Salisbury, J. L. (1988) Identification and localization of a novel, cytoskeletal, centrosome-associated protein in PtK2 cells. *J. Cell Biol.* **107,** 2669–2678 CrossRef Medline
5. Paoletti, A., Moudjou, M., Paintrand, M., Salisbury, J. L., and Bornens, M. (1996) Most of centrin in animal cells is not centrosome-associated and centrosomal centrin is confined to the distal lumen of centrioles. *J. Cell Sci.* **109**, 3089–3102 Medline
6. Salisbury, J. L. (2007) A mechanistic view on the evolutionary origin for centrin-based control of centriole duplication. *J. Cell. Physiol.* **213,** 420–428 CrossRef Medline
7. Dantas, T. J., Daly, O. M., and Morrison, C. G. (2012) Such small hands: The roles of centrins/caltractins in the centriole and in genome maintenance. *Cell. Mol. Life Sci.* **69,** 2979–2997 CrossRef Medline
8. Schiebel, E., and Bornens, M. (1995) In search of a function for centrins. *Trends Cell Biol.* **5,** 197–201 CrossRef Medline
9. Dantas, T. J., Wang, Y., Lalor, P., Dockery, P., and Morrison, C. G. (2011) Defective nucleotide excision repair with normal centrosome structures and functions in the absence of all vertebrate centrins. *J. Cell Biol.* **193,** 307–318 CrossRef Medline
10. Salisbury, J. L., Suino, K. M., Busby, R., and Springett, M. (2002) Centrin-2 is required for centriole duplication in mammalian cells. *Curr. Biol.* **12,** 1287–1292 CrossRef Medline
11. Strnad, P., Leidel, S., Vinogradova, T., Euteneuer, U., Khodjakov, A., and Gönczy, P. (2007) Regulated HsSAS-6 levels ensure formation of a single procentriole per centriole during the centrosome duplication cycle. *Dev. Cell* **13,** 203–213 CrossRef Medline
12. Yang, C. H., Kasbek, C., Majumder, S., Yusof, A. M., and Fisk, H. A. (2010) Mps1 phosphorylation sites regulate the function of centrin 2 in centriole assembly. *Mol. Biol. Cell* **21,** 4361–4372 CrossRef Medline
13. Kleylein-Sohn, J., Westendorf, J., Le Clech, M., Habedanck, R., Stierhof, Y. D., and Nigg, E. A. (2007) Plk4-induced centriole biogenesis in human cells. *Dev. Cell* **13,** 190–202 CrossRef Medline
14. Middendorp, S., Küntziger, T., Abraham, Y., Holmes, S., Bordes, N., Paintrand, M., Paoletti, A., and Bornens, M. (2000) A role for centrin 3 in centrosome reproduction. *J. Cell Biol.* **148,** 405–416 CrossRef Medline
15. Prosser, S. L., and Morrison, C. G. (2015) Centrin2 regulates CP110 removal in primary cilium formation. *J. Cell Biol.* **208,** 693–701 CrossRef Medline
16. Delaval, B., Covassin, L., Lawson, N. D., and Doxsey, S. (2011) Centrin depletion causes cyst formation and other ciliopathy-related phenotypes in zebrafish. *Cell Cycle* **10,** 3964–3972 CrossRef Medline
17. Friedberg, F. (2006) Centrin isoforms in mammals: Relation to calmodulin. *Mol. Biol. Rep.* **33,** 243–252 CrossRef Medline
18. Bornens, M., and Azimzadeh, J. (2007) Origin and evolution of the centrosome. *Adv. Exp. Med. Biol.* **607,** 119–129 CrossRef Medline
19. Hart, P. E., Glantz, J. N., Orth, J. D., Poynter, G. M., and Salisbury, J. L. (1999) Testis-specific murine centrin, Cetn1: Genomic characterization and evidence for retroposition of a gene encoding a centrosome protein. *Genomics* **60,** 111–120 CrossRef Medline
20. Middendorp, S., Paoletti, A., Schiebel, E., and Bornens, M. (1997) Identification of a new mammalian centrin gene, more closely related to *Saccharomyces cerevisiae* CDC31 gene. *Proc. Natl. Acad. Sci. U.S.A.* **94,** 9141–9146 CrossRef Medline
21. Gavet, O., Alvarez, C., Gaspar, P., and Bornens, M. (2003) Centrin4p, a novel mammalian centrin specifically expressed in ciliated cells. *Mol. Biol. Cell* **14,** 1818–1834 CrossRef Medline
22. Avasthi, P., Scheel, J. F., Ying, G., Frederick, J. M., Baehr, W., and Wolfrum, U. (2013) Germline deletion of Cetn1 causes infertility in male mice. *J. Cell Sci.* **126,** 3204–3213 CrossRef Medline
23. Ying, G., Avasthi, P., Irwin, M., Gerstner, C. D., Frederick, J. M., Lucero, M. T., and Baehr, W. (2014) Centrin 2 is required for mouse olfactory ciliary trafficking and development of ependymal cilia planar polarity. *J. Neurosci.* **34,** 6377–6388 CrossRef Medline
24. Giessl, A., Pulvermüller, A., Trojan, P., Park, J. H., Choe, H. W., Ernst, O. P., Hofmann, K. P., and Wolfrum, U. (2004) Differential expression and interaction with the visual G-protein transducin of centrin isoforms in mammalian photoreceptor cells. *J. Biol. Chem.* **279,** 51472–51481 CrossRef Medline
25. Pulvermüller, A., Giessl, A., Heck, M., Wottrich, R., Schmitt, A., Ernst, O. P., Choe, H. W., Hofmann, K. P., and Wolfrum, U. (2002) Calcium-dependent assembly of centrin-G-protein complex in photoreceptor cells. *Mol. Cell. Biol.* **22,** 2194–2203 CrossRef Medline
26. Dharmat, R., Eblimit, A., Robichaux, M. A., Zhang, Z., Nguyen, T. T., Jung, S. Y., He, F., Jain, A., Li, Y., Qin, J., Overbeek, P., Roepman, R., Mardon, G., Wensel, T. G., and Chen, R. (2018) SPATA7 maintains a novel photoreceptor-specific zone in the distal connecting cilium. *J. Cell Biol.* **217,** 2851–2865 CrossRef Medline
27. Liu, Q., Zuo, J., and Pierce, E. A. (2004) The retinitis pigmentosa 1 protein is a photoreceptor microtubule-associated protein. *J. Neurosci.* **24,** 6427–6436 CrossRef Medline
28. Liu, Q., Lyubarsky, A., Skalet, J. H., Pugh, E. N., Jr, and Pierce, E. A. (2003) RP1 is required for the correct stacking of outer segment discs. *Invest. Ophthalmol. Vis. Sci.* **44,** 4171–4183 CrossRef Medline
29. Gao, J., Cheon, K., Nusinowitz, S., Liu, Q., Bei, D., Atkins, K., Azimi, A., Daiger, S. P., Farber, D. B., Heckenlively, J. R., Pierce, E. A., Sullivan, L. S., and Zuo, J. (2002) Progressive photoreceptor degeneration, outer segment dysplasia, and rhodopsin mislocalization in mice with targeted disruption of the retinitis pigmentosa-1 (*Rp1*) gene. *Proc. Natl. Acad. Sci. U.S.A.* **99,** 5698–5703 CrossRef Medline
30. Stuck, M. W., Conley, S. M., and Naash, M. I. (2016) PRPH2/RDS and ROM-1: Historical context, current views and future considerations. *Prog. Retin. Eye Res.* **52,** 47–63 CrossRef Medline
31. Yang, Z., Chen, Y., Lillo, C., Chien, J., Yu, Z., Michaelides, M., Klein, M., Howes, K. A., Li, Y., Kaminoh, Y., Chen, H., Zhao, C., Al-Sheikh, Y. T., Karan, G., Corbeil, D., *et al.* (2008) Mutant prominin 1 found in patients with macular degeneration disrupts photoreceptor disk morphogenesis in mice. *J. Clin. Invest.* **118,** 2908–2916 Medline
32. Sharif, A. S., Yu, D., Loertscher, S., Austin, R., Nguyen, K., Mathur, P. D., Clark, A. M., Zou, J., Lobanova, E. S., Arshavsky, V. Y., and Yang, J. (2018) C8ORF37 is required for photoreceptor outer segment disc morphogenesis by maintaining outer segment membrane protein homeostasis. *J. Neurosci.* **38,** 3160–3176 CrossRef Medline
33. Sedmak, T., and Wolfrum, U. (2010) Intraflagellar transport molecules in ciliary and nonciliary cells of the retina. *J. Cell Biol.* **189,** 171–186 CrossRef Medline
34. Baum, P., Furlong, C., and Byers, B. (1986) Yeast gene required for spindle pole body duplication: homology of its product with Ca2+-binding proteins. *Proc. Natl. Acad. Sci. U.S.A.* **83,** 5512–5516 CrossRef Medline
35. Marshall, W. F., Vucica, Y., and Rosenbaum, J. L. (2001) Kinetics and regulation of *de novo* centriole assembly: Implications for the mechanism of centriole duplication. *Curr. Biol.* **11,** 308–317 CrossRef Medline
36. Koblenz, B., Schoppmeier, J., Grunow, A., and Lechtreck, K. F. (2003) Centrin deficiency in *Chlamydomonas* causes defects in basal body replication, segregation and maturation. *J. Cell Sci.* **116,** 2635–2646 CrossRef Medline
37. Davis, E. E., and Katsanis, N. (2012) The ciliopathies: a transitional model into systems biology of human genetic disease. *Curr. Opin. Genet. Dev.* **22,** 290–303 CrossRef Medline
38. Kim, G. W., Li, L., Ghorbani, M., You, L., and Yang, X. J. (2013) Mice lacking α-tubulin acetyltransferase 1 are viable but display α-tubulin acetylation deficiency and dentate gyrus distortion. *J. Biol. Chem.* **288,** 20334–20350 CrossRef Medline
39. Xu, Z., Schaedel, L., Portran, D., Aguilar, A., Gaillard, J., Marinkovich, M. P., Théry, M., and Nachury, M. V. (2017) Microtubules acquire resistance from mechanical breakage through intralumenal acetylation. *Science* **356,** 328–332 CrossRef Medline
40. Portran, D., Schaedel, L., Xu, Z., Théry, M., and Nachury, M. V. (2017) Tubulin acetylation protects long-lived microtubules against mechanical ageing. *Nat. Cell Biol.* **19,** 391–398 CrossRef Medline
41. Bicek, A. D., Tüzel, E., Demtchouk, A., Uppalapati, M., Hancock, W. O., Kroll, D. M., and Odde, D. J. (2009) Anterograde microtubule transport drives microtubule bending in LLC-PK1 epithelial cells. *Mol. Biol. Cell* **20,** 2943–2953 CrossRef Medline

42. Robison, P., Caporizzo, M. A., Ahmadzadeh, H., Bogush, A. I., Chen, C. Y., Margulies, K. B., Shenoy, V. B., and Prosser, B. L. (2016) Detyrosinated microtubules buckle and bear load in contracting cardiomyocytes. *Science* **352,** aaf0659 CrossRef Medline
43. Brangwynne, C. P., MacKintosh, F. C., Kumar, S., Geisse, N. A., Talbot, J., Mahadevan, L., Parker, K. K., Ingber, D. E., and Weitz, D. A. (2006) Microtubules can bear enhanced compressive loads in living cells because of lateral reinforcement. *J. Cell Biol.* **173,** 733–741 CrossRef Medline
44. Shida, T., Cueva, J. G., Xu, Z., Goodman, M. B., and Nachury, M. V. (2010) The major α-tubulin K40 acetyltransferase αTAT1 promotes rapid ciliogenesis and efficient mechanosensation. *Proc. Natl. Acad. Sci. U.S.A.* **107,** 21517–21522 CrossRef Medline
45. Pugacheva, E. N., Jablonski, S. A., Hartman, T. R., Henske, E. P., and Golemis, E. A. (2007) HEF1-dependent Aurora A activation induces disassembly of the primary cilium. *Cell* **129,** 1351–1363 CrossRef Medline
46. Eblimit, A., Nguyen, T. M., Chen, Y., Esteve-Rudd, J., Zhong, H., Letteboer, S., Van Reeuwijk, J., Simons, D. L., Ding, Q., Wu, K. M., Li, Y., Van Beersum, S., Moayedi, Y., Xu, H., Pickard, P., *et al.* (2015) *Spata7* is a retinal ciliopathy gene critical for correct RPGRIP1 localization and protein trafficking in the retina. *Hum. Mol. Genet.* **24,** 1584–1601 CrossRef Medline
47. Karlstetter, M., Sorusch, N., Caramoy, A., Dannhausen, K., Aslanidis, A., Fauser, S., Boesl, M. R., Nagel-Wolfrum, K., Tamm, E. R., Jägle, H., Stoehr, H., Wolfrum, U., and Langmann, T. (2014) Disruption of the retinitis pigmentosa 28 gene *Fam161a* in mice affects photoreceptor ciliary structure and leads to progressive retinal degeneration. *Hum. Mol. Genet.* **23,** 5197–5210 CrossRef Medline
48. Mattapallil, M. J., Wawrousek, E. F., Chan, C. C., Zhao, H., Roychoudhury, J., Ferguson, T. A., and Caspi, R. R. (2012) The Rd8 mutation of the *Crb1* gene is present in vendor lines of C57BL/6N mice and embryonic stem cells, and confounds ocular induced mutant phenotypes. *Invest. Ophthalmol. Vis. Sci.* **53,** 2921–2927 CrossRef Medline
49. Wu, S., Ying, G., Wu, Q., and Capecchi, M. R. (2008) A protocol for constructing gene targeting vectors: Generating knockout mice for the cadherin family and beyond. *Nat. Protoc.* **3,** 1056–1076 CrossRef Medline
50. Truett, G. E., Heeger, P., Mynatt, R. L., Truett, A. A., Walker, J. A., and Warman, M. L. (2000) Preparation of PCR-quality mouse genomic DNA with hot sodium hydroxide and Tris (HotSHOT). *Biotechniques* ***29,*** **52,** 54 Medline
51. Coleman, J. A., Zhu, X., Djajadi, H. R., Molday, L. L., Smith, R. S., Libby, R. T., John, S. W., and Molday, R. S. (2014) Phospholipid flippase ATP8A2 is required for normal visual and auditory function and photoreceptor and spiral ganglion cell survival. *J. Cell Sci.* **127,** 1138–1149 CrossRef Medline
52. Ying, G., Gerstner, C. D., Frederick, J. M., Boye, S. L., Hauswirth, W. W., and Baehr, W. (2016) Small GTPases Rab8a and Rab11a are dispensable for rhodopsin transport in mouse photoreceptors. *PLoS ONE* **11,** e0161236 CrossRef Medline
53. Zhu, X., Li, A., Brown, B., Weiss, E. R., Osawa, S., and Craft, C. M. (2002) Mouse cone arrestin expression pattern: Light induced translocation in cone photoreceptors. *Mol. Vis.* **8,** 462–471 Medline
54. Chang, B., Khanna, H., Hawes, N., Jimeno, D., He, S., Lillo, C., Parapuram, S. K., Cheng, H., Scott, A., Hurd, R. E., Sayer, J. A., Otto, E. A., Attanasio, M., O'Toole, J. F., Jin, G., *et al.* (2006) In-frame deletion in a novel centrosomal/ciliary protein CEP290/NPHP6 perturbs its interaction with RPGR and results in early-onset retinal degeneration in the rd16 mouse. *Hum. Mol. Genet.* **15,** 1847–1857 CrossRef Medline
55. Hong, D. H., Pawlyk, B. S., Shang, J., Sandberg, M. A., Berson, E. L., and Li, T. (2000) A retinitis pigmentosa GTPase regulator (RPGR)-deficient mouse model for X-linked retinitis pigmentosa (RP3). *Proc. Natl. Acad. Sci. U.S.A.* **97,** 3649–3654 CrossRef Medline
56. Hong, D. H., Yue, G., Adamian, M., and Li, T. (2001) Retinitis pigmentosa GTPase regulator (RPGR)-interacting protein is stably associated with the photoreceptor ciliary axoneme and anchors RPGR to the connecting cilium. *J. Biol. Chem.* **276,** 12091–12099 CrossRef Medline
57. MacKenzie, D., Arendt, A., Hargrave, P., McDowell, J. H., and Molday, R. S. (1984) Localization of binding sites for carboxyl terminal specific anti-rhodopsin monoclonal antibodies using synthetic peptides. *Biochemistry* (*Mosc.*) **23,** 6544–6549 CrossRef Medline
58. Moritz, O. L., and Molday, R. S. (1996) Molecular cloning, membrane topology, and localization of bovine rom-1 in rod and cone photoreceptor cells. *Invest. Ophthalmol. Vis. Sci.* **37,** 352–362 Medline
59. Molday, R. S., Hicks, D., and Molday, L. (1987) Peripherin: A rim-specific membrane protein of rod outer segment discs. *Invest. Ophthalmol. Vis. Sci.* **28,** 50–61 Medline
60. Haire, S. E., Pang, J., Boye, S. L., Sokal, I., Craft, C. M., Palczewski, K., Hauswirth, W. W., and Semple-Rowland, S. L. (2006) Light-driven cone arrestin translocation in cones of postnatal guanylate cyclase-1 knockout mouse retina treated with AAV-GC1. *Invest. Ophthalmol. Vis. Sci.* **47,** 3745–3753 CrossRef Medline
61. Liu, Q., Zhou, J., Daiger, S. P., Farber, D. B., Heckenlively, J. R., Smith, J. E., Sullivan, L. S., Zuo, J., Milam, A. H., and Pierce, E. A. (2002) Identification and subcellular localization of the RP1 protein in human and mouse photoreceptors. *Invest. Ophthalmol. Vis. Sci.* **43,** 22–32 Medline
62. Rachel, R. A., May-Simera, H. L., Veleri, S., Gotoh, N., Choi, B. Y., Murga-Zamalloa, C., McIntyre, J. C., Marek, J., Lopez, I., Hackett, A. N., Zhang, J., Brooks, M., den Hollander, A. I., Beales, P. L., Li, T., *et al.* (2012) Combining Cep290 and Mkks ciliopathy alleles in mice rescues sensory defects and restores ciliogenesis. *J. Clin. Invest.* **122,** 1233–1245 CrossRef Medline
63. Weigmann, A., Corbeil, D., Hellwig, A., and Huttner, W. B. (1997) Prominin, a novel microvilli-specific polytopic membrane protein of the apical surface of epithelial cells, is targeted to plasmalemmal protrusions of non-epithelial cells. *Proc. Natl. Acad. Sci. U.S.A.* **94,** 12425–12430 CrossRef Medline
64. Pazour, G. J., Baker, S. A., Deane, J. A., Cole, D. G., Dickert, B. L., Rosenbaum, J. L., Witman, G. B., and Besharse, J. C. (2002) The intraflagellar transport protein, IFT88, is essential for vertebrate photoreceptor assembly and maintenance. *J. Cell Biol.* **157,** 103–113 CrossRef Medline